X-ray and Neutron Structure Determination and Magnetic Properties of New Quaternary Phases $RE_{0.67}Ni_2Ga_{5+n-x}Ge_x$ and $RE_{0.67}Ni_2Ga_{5+n-x}Si_x$ (n = 0, 1; RE = Y, Sm, Gd, Tb, Dy, Ho, Er, Tm) Synthesized in Liquid Ga

Marina A. Zhuravleva,[†] X. Z. Chen,[†] Xiaoping Wang,[‡] Arthur J. Schultz,[‡] John Ireland,[§] Carl K. Kannewurf,[§] and Mercouri G. Kanatzidis*[,†]

Department of Chemistry, Michigan State University, East Lansing, Michigan 48824, Department of Electrical Engineering and Computer Science, Northwestern University, Evanston, Illinois 60208, and Intense Pulsed Neutron Source, Argonne National Laboratory, Argonne, Illinois 60439

Received February 1, 2002. Revised Manuscript Received May 2, 2002

Liquid Ga was used as a solvent to explore the phase formation between rare-earth metals (REs), Ni, and a tetrelide (Tt = Si, Ge). The reactions were performed in excess liquid Ga at 850 °C. Two new phases of general formulas $RE_{0.67}Ni_2Ga_{5-x}Tt_x$ and $RE_{0.67}Ni_2Ga_{6-x}Tt_x$ were found and structurally characterized. The Co analogues of the latter $RE_{0.67}Co_2Ga_{6-x}Ge_x$ (RE = Y, Gd) were also prepared. Single-crystal X-ray data: The first group of compounds $RE_{0.67}Ni_2Ga_{5-x}Tt_x$ crystallizes in the hexagonal space group $P6_3/mmc$ with a structure related to the $RE_{2-x}Pt_4Ga_{8+y}$ type ($Sm_{0.53}Ni_2Ga_{5-x}Ge_x$, a = 4.1748(7) Å, c = 16.007(4) Å, V = 241.61(8) Å^3, Z = 2; $Y_{0.59}Ni_2Ga_{5-x}Ge_x$, a = 4.1344(11) Å, c = 15.887(6) Å, V = 235.18(12) Å^3, Z = 2; $Tb_{0.67}Ni_2Ga_{5-x}Si_x$, a = 4.1415(11) Å, c = 15.843(6) Å, V = 235.33(12) Å^3, Z = 2; $Ho_{0.67}Ni_2Ga_{5-x}Ge_x$, a = 4.1491(4) Å, c = 15.877(2) Å, V = 236.71(5) Å^3, Z = 2). The second group $RE_{0.67}Ni_2Ga_{6-x}Tt_x$ crystallizes in $P\bar{6}m2$ ($Gd_{0.67}Ni_2Ga_{6-x}Ge_x$, a = 4.1856(10) Å, c = 9.167(3) Å, V = 139.08(7) Å^3, Z = 1; $Sm_{0.67}Ni_2Ga_{6-x}Si_x$, a = 4.1976(8) Å, c = 9.159(3) Å, V = 139.76(5) Å^3, Z = 1) in a structure related to the $ErNi_3Al_9$ structure type with disorder in the RE−Ga plane. $Dy_{0.67}Ni_2Ga_{6-x}Ge_x$ crystallizes in space group $P\bar{3}1c$ (a = 7.2536(8) Å, c = 18.308(3) Å, V = 834.21(2) Å^3, Z = 6) with partial disorder in the RE−Ga plane. The structures of these two groups of compounds are related to each other and contain similar building motifs, namely $Ga_n[NiGa_{2-x/2}Ge_{x/2}]_2$ slabs and $RE_{0.67}Ga$ monatomic layers which alternate along the c-direction, forming a 3D structure. The parameter x and the position of the tetrelide in the structure were determined by single-crystal neutron diffraction. Complete or partial disorder of the RE and Ga atoms is observed in the RE−Ga plane. The origin of the disorder lies in the extensive and random stacking faults of ordered RE−Ga planes, which apparently slide easily in the *ab* plane and create an averaged disordered picture. Electrical conductivity and thermopower measurements indicate that these compounds are metallic conductors. The magnetic measurements show antiferromagnetic ordering at ∼3−4 K and Curie−Weiss behavior at higher temperatures with the values of μ_{eff} close to those of RE^{3+} free ions. Strong 2-fold crystal field anisotropy is observed for the heavy RE analogues. The anisotropy constants K_2^{para} calculated from the Weiss constant anisotropy for heavy RE analogues are reported.

Introduction

The use of liquid Al as a reactive solvent to prepare silicon-containing intermetallic compounds has been recently demonstrated in the discovery of several novel systems such as $Sm_2Ni(Ni_xSi_{1-x})Al_4Si_6$,[1] $Ln_2Al_3Si_2$,[2] and $RE_8Ru_{12}Al_{49}Si_9(Al_xSi_{12-x})$.[3] In this approach, different elements—rare-earth metals, transitional metals, and silicon—are allowed to react in the molten Al medium at much lower temperatures than typically employed in the synthesis of compounds of this type. A remarkable property that has emerged so far from these studies is that Al always gets incorporated into the products, giving rise to an interesting class of compounds, namely complex *metal aluminum silicides*. Therefore, Al acts both as a solvent and as a reagent. When we employed liquid Ga to perform similar reaction chemistry in the corresponding systems RE/M/Ga/Si (RE = rare-earth metal, M = transition metal), we noticed that it was

* To whom correspondence should be addressed.
[†] Michigan State University.
[‡] Argonne National Laboratory.
[§] Northwestern University.

(1) Chen, X. Z.; Sportouch, S.; Brazis, P.; Kannewurf, C. R.; Cowen, J. A.; Patschke, R.; Kanatzidis, M. G. *Chem. Mater.* **1998**, *10*, 3202.
(2) Chen, X. Z.; Sieve, B.; Henning, R.; Schultz, A. J.; Brazis, P.; Kannewurf, C. R.; Cowen, J. A.; Crosby, R.; Kanatzidis, M. G. *Angew. Chem., Intl. Ed. Engl.* **1999**, *38*, 693.
(3) Sieve, B.; Chen, X. Z.; Henning, R.; Brazis, P.; Kannevurf, C. R.; Cowen, J. A.; Schultz, A. J.; Kanatzidis, M. G. *J. Am. Chem. Soc.* **2001**, *29*, 7040.

10.1021/cm020066o CCC: $22.00
Published on Web 06/25/2002

considerably more difficult to incorporate Ga in the products. A general tendency to separate into ternary RE/M/Si and RE/Ga/Si phases was observed. For example, the system Sm/Ni/Ga/Si (where the Sm/Ni ratio was >1) readily gave rise to $SmNiSi_3$[4] and Sm_2NiGa_{12}[5] phases, whereas under identical conditions the corresponding system Sm/Ni/Al/Si results in $Sm_2Ni(Ni_xSi_{1-x})Al_4Si_6$. Since Ga and Al are isoelectronic and have similar sizes, it is hard to explain the above bifurcation in their chemistry, especially when the solubility of Si in Al is similar to that in Ga.[6] For this reason, we decided to study the Ga systems in more detail and also to compare and contrast the chemistry of Ge analogues vis-à-vis Si. Remarkably, we find that the RE/M/Ga/Ge systems promptly proceed to give quaternary compounds regardless of the RE/M ratio (for example the RE/Ni/Ga/Si system produced quaternaries only when RE/Ni < 1). Among the RE/Ni/Ga/Ge systems with different transition metals M, the one with M = Ni was studied in more detail in order to contrast it to the corresponding RE/Ni/Ga/Si. The related system with M = Co is also of interest; however, fewer investigations with it have been performed. Nevertheless, we find similar tendencies to those of Ni with several isostructural analogues. Here we report the synthesis, structure, and physical properties of two new types of quaternary compounds of the homologous series $RE_{0.67}Ni_2Ga_{5+n-x}Tt_x$ (n = 0; 1): $RE_{0.67}Ni_2Ga_{5-x}Si_x$ (RE = Y, Sm, Gd, Tb); $RE_{0.67}Ni_2Ga_{5-x}Ge_x$ (RE = Y, Sm, Gd, Tb, Er Ho, Tm); $RE_{0.67}Ni_2Ga_{6-x}Si_x$ (RE = Y, Sm, Gd); $RE_{0.67}Ni_2Ga_{6-x}Ge_x$ (RE = Y, Sm, Gd, Dy); and $RE_{0.67}Co_2Ga_{6-x}Ge_x$ (RE = Y, Gd).

Experimental Section

Synthesis. The reactions between the rare-earth element, nickel, and a tetrelide (Tt = Si, Ge), taken in the ratio RE/Ni/Ga/T 1:2:30:2, were performed in liquid Ga as a reactive solvent at 850 °C. The elemental rare-earth (Y, Sm, Dy, Gd, Tb, Er, Ho, Tm), typically of purity 99.9% (CERAC Inc.), nickel powder 99.99% (Aldrich Inc.), Ge powder (99.999%, CERAC Inc.), Si powder (99.999%, CERAC Inc.), and Ga (3 mm shots 99.999%, CERAC Inc.) were taken in the following amounts—RE, 1.2 mmol; Ni, 2.4 mmol; Ga, 36 mmol; Ge(Si), 2.4 mmol—and loaded into alumina crucibles under an inert (N_2) atmosphere. The crucibles were placed into fused silica tubes, sealed under vacuum ($\sim 1 \times 10^{-4}$ Torr) and subjected to the following treatment: they were heated to 1000 °C at the rate 60 deg/h, kept at 1000 °C for 5 h to allow proper homogenization, cooled to 850 °C in 2 h, and kept isothermally at 850 °C for 3 days and then slowly cooled to 200 °C at the rate 18 deg/h and, finally, to 50 °C in 2 h. The products were removed from the crucibles with hot water. The excess Ga was filtered through a coarse frit by centrifuging at 250 °C. The residual Ga was removed using an ~5 M solution of iodine in DMF over 12 h at room temperature. The resulting crystalline product was subsequently washed in DMF and dried with acetone and ether.

Elemental Analysis and X-ray Powder Diffraction. The chemical composition of the products was determined by energy dispersive spectroscopy (EDS) performed on a scanning electron microscope (SEM) JEOL JSM-35C equipped with an EDS detector. The analysis was conducted at the accelerating voltage 20 kV and collection time 30 s. Several samples from each batch were analyzed, and the results were averaged.

The X-ray diffraction (XRD) powder patterns of products were taken at room temperature on a Rigaku-Denki/Rw400F2 (rotaflex) rotating-anode (Cu Kα) powder diffractometer and a CPS 120 INEL X-ray diffractometer (Cu Kα) equipped with a position-sensitive detector. Experimental powder patterns were compared to that calculated from single-crystal data using the CERIUS[2] software package.[7]

RE/M/Ga/Ge Phase Composition (M = Ni, Co). The reaction between RE/Ni/Ga/Ge (RE = Y, Sm, Gd, Tb, Er, Ho, Tm) produced predominately a new quaternary phase $RE_{0.67}Ni_2Ga_{5-x}Ge_x$ (**1**) with elemental composition $RE_{0.67}Ni_2Ga_{3.5}Ge_{0.8}$, as determined by EDS. More than 90% of the Bragg peaks of the XRD pattern were attributed to **1**, and less than 10% were due to recrystallized but unreacted Ge. Another more Ga-rich phase $RE_{0.67}M_2Ga_{6-x}Ge_x$ (**2**) was found in the systems Gd/Ni/Ga/Ge, Gd/Co/Ga/Ge, Y/Ni/Ga/Ge, Y/Co/Ca/Ge, and Dy/Ni/Ga/Ge, although a high yield (>90%) was observed only for the two latter ones. For some RE analogues of **1** and **2**, the formation of an additional binary Ni−Ga side product was detected with EDS analysis. This side phase forms on the surface of the crystals of quaternary phases. The presence of the Ni−Ga binary phases was not detected with powder diffraction because of the minor quantities or lack of crystallinity. To reduce the formation of the undesirable Ni−Ga side-phase, we used higher than stoichiometric amounts of Ge in order to shift the reaction equilibrium toward the formation of quaternary phases.

RE/Ni/Ga/Si Phase Composition. The products of the reaction conducted under similar conditions in the RE/Ni/Ga/Si system are very different from those of the RE/Ni/Ga/Ge system. The XRD patterns show a multiphase composition which varies from rare-earth to rare-earth and includes phases **1** and **2**, the ternary phases $RENiSi_3$,[4] $RE_2Ni_3Si_5$, and NiGaSi,[8] the binary Ni−Ga, and Si. The yield of the quaternary phases was studied as a function of the duration of the isothermal step, the cooling rate, and the flux amount. The maximal yield of 50/50% for the quaternary phases **1** and **2** was observed for Sm/Ni/Ga/Si under the synthesis conditions indicated in the Synthesis section.

X-ray Crystallography. Single crystals of the four isotypic compounds of **1** (RE = Y, Sm, Ho with Tt = Ge; and RE = Tb with Tt = Si) and three analogues of **2** (RE = Dy, Gd with Tt = Ge; and RE = Sm with Tt = Si) were mounted on glass fibers. The crystallographic data corresponding to a hemisphere or full sphere of reciprocal space were collected on a Siemens Platform SMART CCD diffractometer using a crystal monochromator and Mo Kα (λ = 0.710 73 Å) radiation. The SMART[9] software was used for data acquisition and cell reduction, and the integration was done with the SAINT[10] software package. The face-indexing routine was applied for analytical absorption corrections. The empirical absorption corrections were done using SADABS.[11] The structure solution and refinement were done by direct methods with the SHELXTL[12] software package. The setting of the cell was standardized with the STRUCTURE TIDY program.[13]

The $RE_{0.67}Ni_2Ga_{5-x}Tt_x$ crystallizes in a primitive cell in hexagonal space group $P6_3/mmc$. There are total of five atomic sites in the structure. The two *4f* ($^1/_3$ $^2/_3$ z) positions were unambiguously assigned to Ni and Ga, and the 2*c* ($^1/_3$ $^2/_3$ $^1/_4$) site was assigned to the RE atom. The *6h* (x $2x$ $^1/_4$) M(1) site can be refined either as Ga or Ge. Likewise, the *4e* (0 0 z) position could either be occupied with Ga or have mixed occupancy M(2) with Ga and a tetrelide (Tt). The interchange

(4) Chen, X. Z.; Larson, P.; Sportouch, S.; Brazis, P.; Mahanti, S. D.; Kannewurf, C. R.; Kanatzidis, M. G. *Chem. Mater.* **1999**, *11*, 75.
(5) Chen, X. Z.; Small, P.; Sportouch, S.; Zhuravleva, M.; Brazis, P.; Kannewurf, C. R.; Kanatzidis, M. G. *Chem. Mater.* **2000**, *12*, 2520.
(6) *Binary Alloy Phase Diagrams*; Massalski, T. B., Editor-in-Chief; American Society for Metals: Metals Park, OH, 1990.
(7) *CERIUS*^{2}, Version 1.6; Molecular Simulations Inc.: Cambridge, England, 1994.
(8) $RE_2Ni_3Si_5$ (*Ibam*), NiGaSi ($F\bar{4}3m$), Ni_3Ga_2 ($P\bar{3}m1$). Unpublished results.
(9) *SMART*, Version 5; Siemens Analytical X-ray Systems, Inc.: Madison, WI, 1998.
(10) *SAINT*, Version 4; Siemens Analytical X-ray Systems, Inc.: Madison, WI, 1994−96.
(11) Scheldrick, G. M. *SADABS*; University of Göttingen: Göttingen, Germany.
(12) Sheldrick, G. M. *SHELXTL*, Version 5.1, 1994; Siemens Analytical X-ray Systems, Inc.: Madison, WI, 1997.
(13) Gelato, L. M.; Parthe, E. *J. Appl. Crystallogr.* **1987**, *20*, 139.

Table 1. Crystal Data and Structure Refinement Details for $RE_{0.67}Ni_2Ga_{5-x}Tt_x$ (RE = Y, Sm, Ho with Tt = Ge; RE = Tb with Tt = Si)

	$Y_{0.59}Ni_2Ga_{5-x}Ge_x$ (**1**)	$Sm_{0.53}Ni_2Ga_{5-x}Ge_x$ (**1**)	$Ho_{0.67}Ni_2Ga_{5-x}Ge_x$ (**1**)	$Tb_{0.67}Ni_2Ga_{5-x}Si_x$ (**1**)
parameter x	0.60	0.44	0.60	0.24
formula wt	520.20	546.97	577.42	561.71
temp (K)	293(2)	293(2)	293(2)	293(2)
wavelength, (Å)	0.71073	0.71073	0.71073	0.71073
space group	$P6_3/mmc$	$P6_3/mmc$	$P6_3/mmc$	$P6_3/mmc$
lattice constants (Å)	a = 4.1344(11)	a = 4.1748(7)	a = 4.1491(4)	a = 4.1415(11)
	c = 15.887(6)	c = 16.007(4)	c = 15.877(2)	c = 15.843(6)
volume, (Å^3)	235.18(12)	241.61(8)	236.71(5)	235.33(12)
Z	2	2	2	2
d_{calc} (g/cm^3)	7.346	7.518	8.101	7.927
absorption coeff (mm^{-1})	43.409	41.484	46.957	44.364
F(000)	469	489	512	500
cryst size (mm^3)	0.12 × 0.06 × 0.02	0.14 × 0.08 × 0.04	0.1 × 0.08 × 0.06	0.10 × 0.10 × 0.04
θ range (deg)	2.56−23.14.	5.09−23.20	6.87−32.55	2.57−27.09
limiting indices	$-4 = h = 4$	$-4 = h = 4$	$-4 = h = 6$	$-3 = h = 5$
	$-4 = k = 4$	$-4 = k = 4$	$-6 = k = 3$	$-5 = k = 5$
	$-17 = l = 17$	$-17 = l = 17$	$-22 = l = 23$	$-19 = l = 18$
reflections collected	1263	1379	1641	1184
unique reflections	89	91	199	129
R_{int}	0.0678	0.0535	0.0524	0.0321
completeness to θ (%)	100.0	98.9	95.7	97.7
refinement method	full-matrix least-squares on F^2	full-matrix least-squares on F^2	full-matrix least-squares on F^2	full-matrix least-squares on F^2
variables	19	19	19	19
goodness-of-fit on F^2	1.133	1.164	1.317	1.374
final R indices [$I > 2\sigma(I)$][a]	R_1 = 0.0314, wR_2 = 0.0739	R_1 = 0.0311, wR_2 = 0.0721	R_1 = 0.0332, wR_2 = 0.0846	R_1 = 0.0292, wR_2 = 0.0838
R indices (all data)	R_1 = 0.0314, wR_2 = 0.0739	R_1 = 0.0320, wR_2 = 0.0724	R_1 = 0.0338, wR_2 = 0.0849	R_1 = 0.0324, wR_2 = 0.0849
extinction coefficient	0.100(11)	0.014(2)	0.057(6)	0.0096(18)
highest resid peak (e/Å^3)	2.035 and −1.008	3.028 and −1.282	3.780 and −2.774	1.053 and −1.307

[a] $R_1 = \sum||F_o| - |F_c||/\sum|F_o|$; $wR_2 = [\sum w\{|F_o| - |F_c|\}^2/\sum w|F_o|^2]^{1/2}$; $w = 1/\sigma^2\{|F_o|\}$.

Table 2. Atomic Coordinates and Equivalent Isotropic Displacement Parameters (× 10^3 Å^2), and the Occupancies for $RE_{0.67}Ni_2Ga_{5-x}Tt_x$ (RE = Ho with Tt = Ge; and RE = Tb with Tt = Si)[a,b]

atom	Wykoff symbol	x	y	z	U_{eq}[c]	occupancy
Ho	2c	$^1/_3$	$^2/_3$	$^1/_4$	7(1)	0.67
Tb	2c	$^1/_3$	$^2/_3$	$^1/_4$	6(1)	0.67
M(1)	6h	0.5393(4)	0.0786(8)	$^1/_4$	10(1)	0.33
M(1)	6h	0.5408(10)	0.0820(20)	$^1/_4$	21(2)	0.33
M(2)	4e	0	0	0.1342(1)	9(1)	0.65(15)/0.35(15)
M(2)	4e	0	0	0.1333(2)	9(1)	0.88(2)/0.12(3)
Ga	4f	$^1/_3$	$^2/_3$	0.0459(1)	7(1)	1.0
Ga	4f	$^1/_3$	$^2/_3$	0.0461(2)	6(1)	1.0
Ni	4f	$^1/_3$	$^2/_3$	0.6091(1)	7(1)	1.0
Ni	4f	$^1/_3$	$^2/_3$	0.6098(2)	7(1)	1.0

[a] The first and second lines correspond to RE = Ho with Tt = Ge and to RE = Tb with Tt = Si, respectively. [b] The M(1) position is occupied with Ga or Ge; the M(2) atomic position is occupied with Ga and Tt; the occupancies given are for Ga/Tt, respectively. [c] U_{eq} is defined as one-third of the trace of the orthogonalized U_{ij} tensor.

of Ga and Tt on the *6h* M(1) position, or introduction of the *4e* M(2) disorder position instead of full occupancy with Ga, brought about only subtle changes in the *R*-values. However, the best convergence factor was obtained when M(1) is occupied with Ga and M(2) has a mixed-occupancy with Ga and Tt (65−88% Ga and 35−12% Tt, respectively, depending on the type of RE metal).

Another type of disorder was observed between the RE and M(1)-type atoms. The symmetry equivalents of the RE atoms at 2c ($^1/_3$ $^2/_3$ $^1/_4$) and the M(1) at 6h (x 2x $^1/_4$) form a monatomic plane at $z = \pm^1/_4$ with a triangular mesh pattern (discussed later). The disorder occurs in a way that every RE atom has three neighboring M(1)$_3$ triangles at the very close distance ~1.4 Å, while the M(1) atoms within the triangles are located ~1.6 Å from each other. Furthermore, the occupancies of the RE and M(1) atoms were lower than the full amount allowed by that specific crystallographic position. For example, the occupancy 33% was obtained for the M(1) site, while the RE site is 67% occupied for RE = Tb and Ho, and only 53% and 59% occupied for RE = Sm and Y, respectively. Details of the data collection and structure refinement are listed in Table 1. The atomic coordinates, occupancies, and isotropic displacement parameters for two analogues of **1** (RE = Ho with Tt = Ge; and RE = Tb with Tt = Si) are given in Table 2. The complete list of the coordinates, the interatomic distances, and the anisotropic displacement parameters for all four analogues is contained in the Supporting Information.

Because of the disorder in the structure and the very similar X-ray scattering powers of Ga and Ge, determination of the location of Ge atoms in the unit cell based on X-ray data was difficult. We employed careful semiquantitative elemental EDS analysis with extensive averaging over several crystals to obtain an accurate composition for **1**. The analytical results showed that the average composition of **1** is $RE_{0.67}Ni_2Ga_{3.5}Tt_{0.8}$. If we suppose that the M(1) site belongs to a Ge atom, and M(2) to a Ga atom, the empirical formula would be $RE_{0.67}Ni_2Ga_4Tt$, which is close to the EDS experimental values. On the contrary, if M(1) = Ga and M(2) is mixed-occupied with Ga and T (65% and 35%), the formula becomes $RE_{0.67}Ni_2Ga_{4.3}T_{0.7}$, which is again comparable to the composition given by EDS. Thus, an independent method capable of distinguishing between Ga and Ge such as neutron scattering had to be employed.

The second compound $RE_{0.67}Ni_2Ga_{6-x}Tt_x$ was refined in a structure type that can be viewed as a subcell of the $ErNi_3Al_9$[23] type with a volume nine times smaller (cell parameters $a'/\sqrt{3}$, $c'/3$). The reason for choosing a subcell for structure description is a disorder, similar to that observed between RE atoms and M(1) atoms in **1**.

The subcell structure solution of **2** was done in the hexagonal space group $P\bar{6}m2$ for the $Gd_{0.67}Ni_2Ga_{6-x}Ge_x$ and $Sm_{0.67}Ni_2Ga_{6-x}Si_x$ analogues. A total of six atomic sites were identified, three of which [2i ($^2/_3$ $^1/_3$ z), 2g (0 0 z), and 1d ($^1/_2$ $^2/_3$ $^1/_2$)] were ascribed to Ga; the other two [2h ($^1/_3$ $^2/_3$ z) and 1a (0 0 0)] were assigned to Ni and RE, respectively. The remaining position

Table 3. Crystal Data and Structure Refinement Details for $RE_{0.67}Ni_2Ga_{6-x}Tt_x$ (Re = Sm with Tt = Si; RE = Gd, Dy with Tt = Ge)

	$Sm_{0.67}Ni_2Ga_{6-x}Si_x$ (**2**)	$Gd_{0.58}Ni_2Ga_{6-x}Ge_x$ (**2**)	$Dy_{0.62}Ni_2Ga_{5.25}Ge$ (**2**)
parameter x	0.06	0.67	
formula wt	633.98	546.97	656.52
temp (K)	293(2)	293(2)	293(2)
wavelength (Å)	0.710 73	0.710 73	0.710 73
space group	$P\bar{6}m2$	$P\bar{6}m2$	$P\bar{3}1c$
lattice constants (Å)	$a = 4.1976(8)$	$a = 4.1856(10)$	$a = 7.2536(8)$
	$c = 9.159(3)$	$c = 9.167(3)$	$c = 18.308(3)$
volume, Z (Å^3)	139.76(5), 1	139.08(7), 1	834.23(19), 6
d_{calc} (g/cm^3)	7.533	7.677	7.841
absorption coeff (mm^{-1})	41.508	43.272	44.986
$F(000)$	283	286	1749
cryst size (mm^3)	0.1 × 0.06 × 0.01	0.14 × 0.1 × 0.06	0.08 × 0.08 × 0.08
θ range (deg)	4.45−30.35	4.45−30.72	6.45−32.51
limiting indices	$-5 = h = 5$	$-5 = h = 6$	$-10 = h = 10$
	$-5 = k = 5$	$-5 = k = 5$	$-10 = k = 9$
	$-12 = l = 12$	$-12 = l = 12$	$-17 = l = 27$
reflections collected	1618	1631	5914
unique reflections	204	207	1530
R_{int}	0.0604	0.0574	0.0775
completeness to θ (%)	97.6	97.6	96.2
refinement method	full-matrix least-squares on F^2	full-matrix least-squares on F^2	full-matrix least-squares on F^2
variables/restraints	22	21	93/1
goodness-of-fit on F^2	1.100	1.095	0.840
final R indices [$I > 2\sigma(I)$]	$R_1 = 0.0233$, $wR_2 = 0.0497$	$R_1 = 0.0268$, $wR_2 = 0.0647$	$R_1 = 0.0487$, $wR_2 = 0.1327$
R indices (all data)	$R_1 = 0.0234$, $wR_2 = 0.0497$	$R_1 = 0.0274$, $wR_2 = 0.0649$	$R_1 = 0.0716$, $wR_2 = 0.1389$
extinction coeff	0.036(3)	0.034(5)	0.000 40(10)
highest residual peak (e/Å^3)	1.248 and −0.802	3.738 and −2.005	3.218 and −3.770

[a] $R_1 = \sum||F_o| - |F_c||/\sum|F_o|$; $wR_2 = [\sum w\{|F_o| - |F_c|\}^2/\sum w|F_o|^2]^{1/2}$; $w = 1/\sigma^2\{|F_o|\}$.

Table 4. Atomic Coordinates and Equivalent Isotropic Displacement Parameters (× 10^3 Å^2), and the Occupancies for $RE_{0.67}Ni_2Ga_{6-x}Tt_x$ (RE = Gd with Tt = Ge; and RE = Sm with Tt = Si)[a,b]

atom	Wykoff symbol	x	y	z	U_{eq}[a]	occupancy
Gd	1*a*	0	0	0	9(1)	0.580(6)
Sm	1*a*	0	0	0	6(1)	0.67
Ni	2*h*	$^1/_3$	$^2/_3$	0.2455(2)	10(1)	1.0
Ni	2*h*	$^1/_3$	$^2/_3$	0.2456(2)	8(1)	1.0
M(1)	3*j*	0.2012(7)	−0.2012(7)	0	22(1)	0.33 (Ge)
M(1)	3*j*	0.2074(5)	−0.2074(5)	0	12(1)	0.33 (Ga)
M(2)	2*i*	$^2/_3$	$^1/_3$	0.2003(2)	14(1)	1.0/0.0
M(2)	2*i*	$^2/_3$	$^1/_3$	0.2025(2)	9(1)	0.972(4)/0.03(2)
Ga(3)	2*g*	0	0	0.3490(2)	12(1)	1.0
Ga(3)	2*g*	0	0	0.3491(2)	9(1)	1.0
Ga(4)	1*d*	$^1/_3$	$^2/_3$	$^1/_2$	15(1)	1.0
Ga(4)	1*d*	$^1/_3$	$^2/_3$	$^1/_2$	11(1)	1.0

[a] The first and second lines correspond to RE = Gd with Tt = Ge and to RE = Sm with Tt = Si, respectively. [b] The M(1) position is occupied with Ga or Ge; the M(2) atomic position is occupied with Ga and Tt; the occupancies given are for Ga/Tt, respectively. [c] $U_{(eq)}$ is defined as one-third of the trace of the orthogonalized U_{ij} tensor.

[3*j* (*x* −*x* 0)] could be occupied with Ga or Ge; however, in contrast to the case for **1**, 3*j* is the only site where Ge can be located without a sensible increase in *R*-values. The structure of **2** has a disorder identical to that for **1** between the RE atoms and the M(1)-type atoms, namely a triangular mesh in the RE−M(1) plane. As is the case for **1**, the distances between M(1)−M(1) and RE−M(1) are too short to allow full occupancy in these sites, and therefore the occupancy parameter was freely refined. As a result, a decrease from full occupancy of the RE and M(1) positions to 67% and 33%, respectively, was observed. If the M(1) site were indeed occupied with Ge, the formula of **2** would be $RE_{0.67}Ni_2Ga_5Ge$, which is close to the one obtained from elemental analysis, $RE_{0.6}Ni_2Ga_{5.3}Ge_{0.8}$. Yet, X-ray diffraction does not provide information to discern between Ga and Ge at M(1).

It is interesting that the Dy analogue of **2**, $Dy_{0.67}Ni_2Ga_{6-x}Ge_x$, shows a higher-order substructure with the cell volume $^2/_3$ of that of a "super-cell" of $ErNi_3Al_9$ (parameters a', $^2/_3c'$) or six times larger than that of other analogues of **2**. The in-plane disorder between RE and M(1) is still observed, however, but to a lesser extent. The details of the structural peculiarities of the subcells and a supercell, as well as their relationship, will be discussed later in the section devoted to the crystal structure. Details of the data collection and structure refinement are given in Table 3, and the atomic coordinates, occupancies, and isotropic displacement parameters for RE = Gd with Tt = Ge and for RE = Sm with Tt = Si are given in Table 4. A complete list of X-ray crystallographic data for all analogues of **2** can be found in the Supporting Information.

Neutron Diffraction. To determine exclusively the nature of M(1) triangles and to locate the tetrelide atoms in the structure, neutron diffraction experiments on single-crystal samples of **1** and **2** were performed. In contrast to the small difference in X-ray scattering lengths (∼3%) between Ga and Ge atoms, the neutron scattering lengths for Ga and Ge atoms differ significantly (∼10%). Thus, neutron diffraction provides a better means for distinguishing these two elements in a crystalline sample.

Diffraction data were collected from single crystals of **1** (RE = Y; Tt = Ge) and **2** (RE = Y; Tt = Ge; M = Co) at the Intense Pulsed Neutron Source (IPNS), Argonne National Laboratory, on the single-crystal diffractometer (SCD). A detailed description of the SCD instrument, data collection, and analysis procedures has been published elsewhere.[14,15] A total of 13 and 18 histograms for compounds **1** and **2**, respectively, were measured at χ and ϕ values suitable to cover a unique octant of reciprocal space. An autoindexing algorithm[16] was used to obtain an initial orientation matrix from the peaks in one histogram. Data were indexed using individual orientation matrixes for each histogram, to allow for any misalignment of the sample. Bragg peaks were integrated in three dimensions about their predicted locations and were corrected for the incident neutron spectrum and detector efficiency. The intensities were corrected for absorption using a local program

Table 5. Neutron Crystal Data and Structural Refinement Parameters for 1

	$Y_{0.67}Ni_2Ga_{5-x}Ge_x$
x	0.67
formula wt (g mol^{-1})	527.19
temp (K)	295
cryst system	hexagonal
space group	$P6_3/mmc$
a (Å)	4.179(1)
c (Å)	15.993(5)
V (Å^3)	241.9(1)
Z	2
d_{calc} (g cm^{-3})	7.24
radiation	neutrons
data collection techn	time-of-flight Laue
$\mu(\lambda)$ (cm^{-1})	$0.640 + 0.107\lambda$
no. of refln ($I > 3\sigma(I)$)	459
no. of parameters refined	29
refinement method	full-matrix least-squares on F
R indices: $R_w(F)$,[a] $R(F)$[b]	0.059, 0.055

[a] $R_w(F) = \{\sum[w(F_o - F_c)^2]/\sum[w(F_o)^2]\}^{1/2}$. [b] $R(F) = \sum||F_o| - |F_c||/\sum|F_o|$.

Table 6. Fractional Coordinates and Site Occupancy of 1

position	Wykoff symbol	x	y	z	occupancy
Y	2*c*	1/3	2/3	1/4	0.67
Ga(1)	6*h*	0.5408(6)	0.0817(12)	1/4	0.33
M(2)	4*e*	0	0	0.133 51(9)	0.67 Ga(2)
	4*e*	0	0	0.133 50(9)	0.33 Ge(2)
Ga(3)	4*f*	1/3	2/3	0.045 90(9)	1.0
Ni	4*f*	1/3	2/3	0.608 97(7)	1.0

ANVRED assuming a crystal of spherical shape. The GSAS software package[17] was used for structural analysis. The refinement was based on F_o using reflections with $|F_o| > 3\sigma(F_o)$. For structure solution, the space group and initial coordinates obtained from the single-crystal X-ray analysis were used.

For compound **1**, two solutions, one based on Y/Ga disorder (M(1) = Ga) and the other one based on Y/Ge disorder (M(1) = Ge), were tested with the use of neutron data. The occupancies were refined to 0.680(6) and 0.320(6) for the Y/Ga model. If Ge instead of Ga atoms were placed in the M(1) 6*h* position, these parameters refined to 0.708(6) for Y and 0.292(6) for Ge, and a higher residual *R*-value was obtained. The result is consistent with Ga atom occupation of the M(1) 6*h* position. The refinement also indicates that the M(2) 4*e* position in **1** contains both Ga and Ge atoms, and their occupancies were refined to 0.69(8) and 0.31(8), respectively. The model, where M(1) = Ga(1) and M(2) = Ga(2) + Ge(2), was included in the final structural refinement. The occupancies were fixed to 2/3 for Y at 2*c* and Ga(2) at 4*e* and to 1/3 for Ga(1) at 6*h* and Ge(2) at 4*e*, respectively (see Table 6). According to this solution, the unit cell composition of **1** is then represented as $Y_{0.67}Ni_2Ga_{4.33}Ge_{0.67}$ ($Z = 2$). The obtained formula is in good agreement with the composition given by the elemental analysis. A summary of parameters related to the neutron diffraction analysis of **1** is given in Table 5. Atomic coordinates and occupancies are listed in Table 6; selected interatomic distances are contained in Table 7.

Because of the close structural relationship of **1** and **2**, we expected to see a similar type of disorder arrangement between Ga and Ge atoms in compound **2** as well. Indeed, the neutron structural refinement for **2** with the best convergence factor corresponds to the model where the M(1) site is occupied with Ga atoms (Ga(1), multiplicity site 3*j*). The Ga(1) atoms are disordered in the same layer with Y atoms with occupancies of 1/3 and 0.60, respectively. Like the tetrelide atoms in **1**, the Ge atoms do not possess any particular crystallographic position in the structure but are disordered with Ga atoms on the same site of multiplicity 2*i*. The mixed occupancy 2*i* site consists of 2/3 Ga(1) and 1/3 Ge(1). The neutron diffraction analysis gave the formula $Y_{0.6}Co_2Ga_{5.33}Ge_{0.67}$ for **2**, which is in very good agreement with the elemental analysis data. For the details of neutron diffraction analysis, see Table 8. The atomic coordinates, occupancies, and selected bond distances are given in Tables 9 and 10.

Table 7. Selected Interatomic Distances (Å) for 1

bond	distance	multiplicity	bond	distance	multiplicity
Y−Ga(1)	1.502(4)	×3	Ga(1)−M(2)	2.815(1)	×4
Y−Ga(1)	2.975(3)	×6	Ni−Ga(3)	2.477(2)	×1
Y−M(2)	3.049(1)	×6	Ni−Ga(3)	2.6151(9)	×3
Y−Ga(3)	3.264(2)	×2	Ni−M(2)	2.4445(7)	×3
Ga(1)−Ga(1)	1.578(8)	×2	Ga(3)−M(2)	2.790(1)	×3
Ga(1)−Ga(1)	2.601(8)	×2	Ga(3)−Ga(3)	2.824(2)	×3
Ga(1)−Ni	2.433(2)	×2			

Table 8. Crystal Data and Structural Refinement Parameters for 2 from Neutron Diffraction

	$Y_{0.60}Co_2Ga_{5.33}Ge_{0.67}$
formula wt (g mol^{-1})	389.859
temp (K)	298(2)
cryst system	hexagonal
space group	$P\bar{6}m2$
a (Å)	4.1822(6)
c (Å)	9.240(2)
V (Å^3)	139.96(4)
Z	1
d_{calc} (g cm^{-3})	6.998
radiation	neutrons
data collection techn	time-of-flight Laue
$\mu(\lambda)$ (cm^{-1})	$0.413 + 0.362\lambda$
reflections ($I > 3\sigma(I)$)	806
parameters refined	39
refinement method	full-matrix least-squares on F
R indices $R_w(F)$,[a] $R(F)$[b]	0.063, 0.048
goodness-of-fit	1.52

[a] $R_w(F) = \{\sum[w(F_o - F_c)^2]/\sum[w(F_o)^2]\}^{1/2}$. [b] $R(F) = \sum||F_o| - |F_c||/\sum|F_o|$.

Physical Properties. A conventional four-probe method and a slow AC technique were used for electrical conductivity and thermopower measurements[18] conducted in the temperature range 4−300 K.

The magnetic susceptibility was measured on single-crystal and polycrystalline samples as a function of temperature in the range 2−400 K in an applied external magnetic field of 500 G with a MPMS Quantum Design Inc. SQUID magnetometer. The field dependence of the magnetic susceptibility was determined at $T = 2$ K in the fields up to ±5 T.

Sample Preparation. The crystals were picked up manually and treated under sonication with *aqua regia*, for about 30 s to eliminate the possible presence of the Ni-containing phases from the surface of the crystals, which could interfere with the magnetic measurements. The crystals were subsequently washed in water, acetone, and ether. Two types of measurements were performed: anisotropic, when crystals with explicit hexagonal rod morphology were placed with the *c*-axis or basal plane parallel to the external magnetic field, and isotropic, using ground polycrystalline samples.

Results and Discussion

Reaction Chemistry. The reactions between rare-earth metal, Ni, and a tetrelide in liquid Ga yielded large, well-formed crystals of the new quaternary phases $RE_{0.67}Ni_2Ga_{5-x}Tt_x$ (Tt = Si, Ge) **(1)**. These crystals have an unusual tapered rod or arrowhead morphology with hexagonal cross-section; see Figure 1. A homologous quaternary compound, $RE_{0.67}Ni_2Ga_{6-x}Tt_x$ **(2)**, with a

(14) Schultz, A. J.; Van Derveer, D. G.; Parker, D. W.; Baldwin, J. E. *Acta Crystallogr., Sect. C* **1990**, *C46*, 276.
(15) Schultz, A. J. *Trans. Am. Crystallogr. Assoc.* **1987**, *23*, 61.
(16) Jacobson, R. A. *J. Appl. Crystallogr.* **1986**, *19*, 283.
(17) Larson, A. C.; Von Dreele, R. B. *GSAS General Structural Analysis System*; Los Alamos National Laboratory, New Mexico, 2000.
(18) Lyding, J. W.; Marcy, H. O.; Marks, T. J.; Kannewurf, C. R. *IEEE Trans. 1nstrum. Meas.* **1988**, *37*, 76.

Table 9. Atomic Coordinates and Site Occupancies for 2

name	Wykoff symbol	*x*	*y*	*z*	occupancy	*U* (eq)
Y	1*a*	0	0	0	0.597(7)	0.0077
Co	2*h*	$^1/_3$	$^2/_3$	0.2440(3)	1.0	0.0105
Ga(1)	3*j*	0.2081(3)	−0.2081(3)	0	0.327(5)	0.0103
M(2)	2*i*	$^2/_3$	$^1/_3$	0.2018(1)	0.67(5) Ga(2)	0.0104
	2*i*	$^2/_3$	$^1/_3$	0.2018(1)	0.33(5) Ge(2)	0.0104
Ga(3)	2*g*	0	0	0.3495(1)	1.0	0.0104
Ga(4)	1*d*	$^1/_3$	$^2/_3$	$^1/_2$	1.0	0.0116

Table 10. Selected Interatomic Distances (Å) for 2

bond	distance	multiplicity	bond	distance	multiplicity
Y−Ga(3)	3.230(1)	×2	Ga(3)−Ga(3)	2.781(2)	×1
Y−M(2)	3.0509(8)	×6	Ga(3)−Ga(4)	2.7864(6)	×3
Y−Ga(1)	2.974(2)	×6	Co−Ga(3)	2.604(1)	×3
Y−Ga(1)	1.508(2)	×3	Co−Ga(4)	2.366(3)	×1
M(2)−Ga(1)	2.8179(8)	×4	Co−M(2)	2.4458(5)	×3
M(2)−Ga(3)	2.7735(7)	×3	Co−Ga(1)	2.430(3)	×2

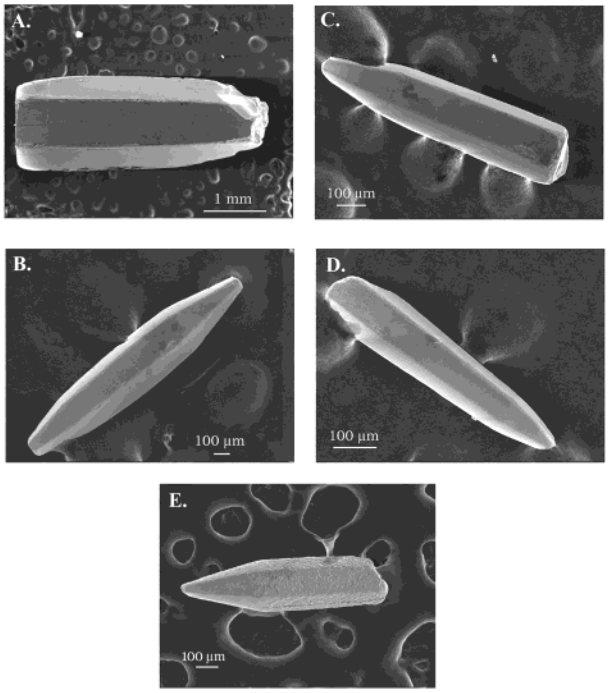

Figure 1. SEM micrographs of crystals of $RE_{0.67}Ni_2Ga_{5-x}Ge_x$: (A and B) $Tm_{0.67}Ni_2Ga_{5-x}Ge_x$; (C and D) $Er_{0.67}Ni_2Ga_{5-x}Ge_x$; (E) $Gd_{0.67}Ni_2Ga_{5-x}Ge_x$.

related structure was first found as a side-phase in the system Sm/Ni/Ga/Si. The $RE_{0.67}Ni_2Ga_{5-x}Tt_x$ phases are very stable and readily form as nearly pure products according to EDS and powder XRD. Originally, the formation of **1** was detected in the Sm/Ni/Al/Si system by its unusual morphology.[19] The isostructural compounds with Y, Sm, and the heavy rare-earth metals (with the exception of Dy, Yb, and Lu) with Si and Ge were obtained. It was found that Ge analogues of **1** form and grow more easily than corresponding Si analogues. For example, the "window" of synthesis conditions is much broader for the Ge analogues; the yield and the crystal size are also higher. It appears to be a general tendency that Ga has a greater "affinity" for Ge than for Si. Thus, in the course of the exploratory investigations in the system RE/Ni/Ga/Tt, we observed predominant formation of the quaternary phases $RE_{0.67}Ni_2Ga_{5-x}Ge_x$ and $RE_3Ni_3Ga_8Ge_3$[20] when Tt = Ge and phase

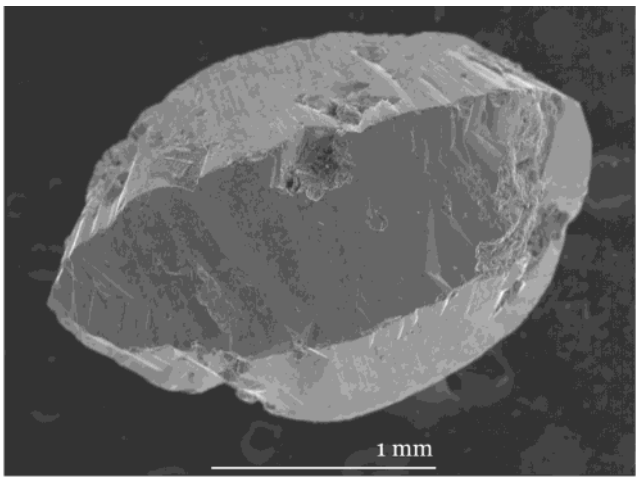

Figure 2. SEM micrograph of a crystal of $Y_{0.67}Co_2Ga_{6-x}Ge_x$.

separation into the ternaries $RENiSi_3$, NiGaSi, and $RE_2Ni_3Si_5$ and the binary Ni_3Ga_2[8] if Tt = Si.

The $RE_{0.67}Ni_2Ga_{6-x}Tt_x$ phase coexists in some cases with the $RE_{0.67}Ni_2Ga_{5-x}Tt_x$ phase, but often as a minor product. The representatives of **2** were found in the systems Sm/Ni/Ga/Si, Y/Ni/Ga/Ge, Gd/Co/Ga/Ge, and Gd/Ni/Ga/Ge in trace amounts, although the conditions under which a single phase of these analogues forms are not yet optimized. However, when the reaction involves Dy, the formation of the otherwise stable phase **1** is suppressed and the formation of **2** is favored. Thus, in the system Dy/Ni/Ga/Ge, nearly a single phase of **2** was obtained under similar conditions to those that yield phases of type **1**. Similarly, in the reaction containing Y/Co/Ga/Ge, a yield of over 95% of **2** was obtained. The morphology of the crystals of **2** varies from chunks with hexagonal faces, as it is for Sm/Ni/Ga/Si, Y/Ni/Ga/Ge, and Gd/Ni/Ga/Ge, to "fat" tapered rods, as it is in the case of Dy/Ni/Ga/Ge and Y/Co/Ga/Ge; see Figure 2.

Crystal Structure of 1: ($Sm_{0.53}Ni_2Ga_{5-x}Ge_x$; $Y_{0.59}Ni_2Ga_{5-x}Ge_x$; $Tb_{0.67}Ni_2Ga_{5-x}Si_x$; $Ho_{0.67}Ni_2Ga_{5-x}Ge_x$). A drawing of **1** ($RE_{0.67}Ni_2Ga_{5-x}Tt_x$; RE = Y; Tt = Ge; x = 0.67) is shown in Figure 3. The larger gray spheres represent Y atoms, and the open circles and the solid circles correspond to Ni and Ga atoms, respectively. The Ga(2)/Ge(2) mixed-occupied M(2) position is shown as spheres with a checkered pattern. The structure of **1** can be viewed as constructed of two types of layers, namely $[NiGa_{2-x/2}Ge_{x/2}]_2$ bilayers and disordered $Y_{0.67}$-Ga(1) monatomic planes; see Figure 3A. The $[NiGa_{2-x/2}Ge_{x/2}]$ layer consists of an arsenic-type layer of M(2) and Ga(3) atoms "stuffed" with Ni atoms;[21,24] see Figure 3B. The Ni−M(2) and Ni−Ga(3) bond distances within the layer are 2.4445(7) and 2.6151(9) Å, respectively; M(2) and Ga(3) are connected at 2.790(1) Å. In this structure, the two single $[NiGa_{2-x/2}Ge_{x/2}]$ layers are joined together

(19) Sieve, B.; Chen, X. Z.; Kanatzidis, M. G. Unpublished results.

(20) Zhuravleva, M.; Kanatzidis, M. G. Unpublished results.

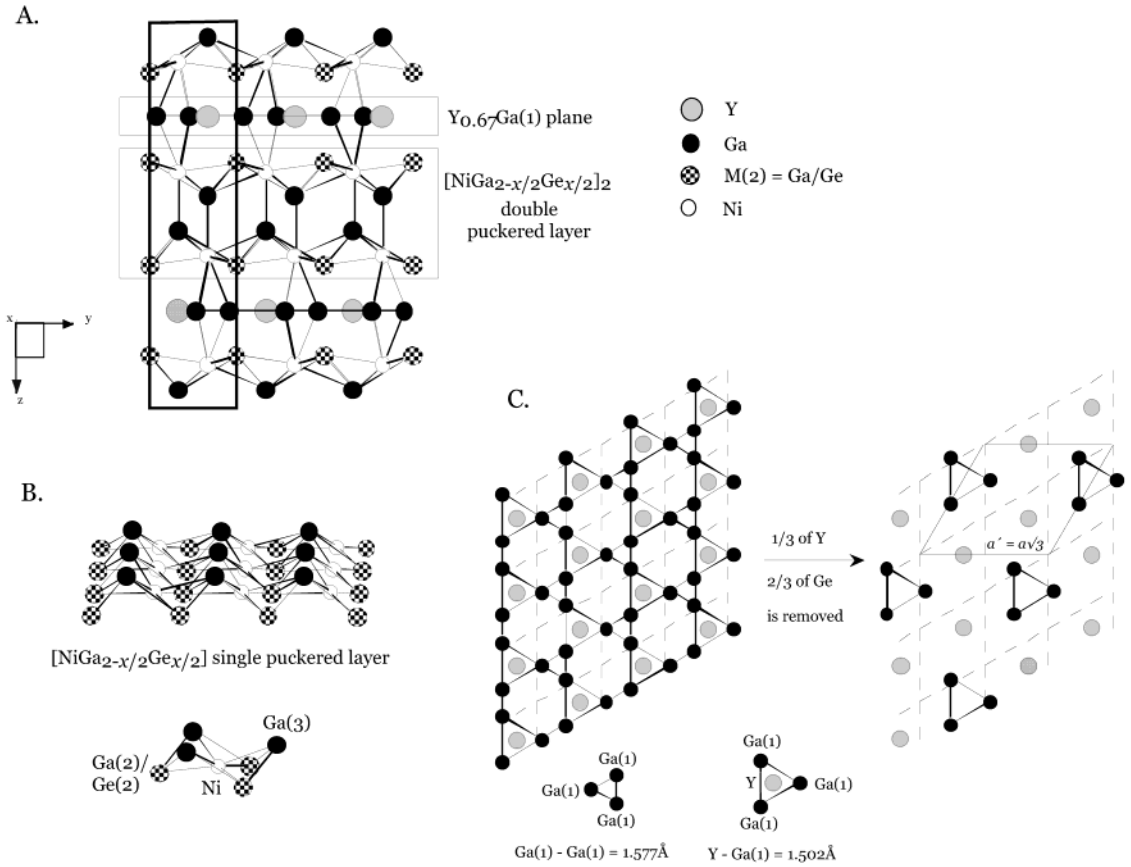

Figure 3. (A) Structure of $Y_{0.67}Ni_2Ga_{5-x}Ge_x$ viewed along the *b*-axis. The black rectangle represents the unit cell. (B) Single $[NiGa_{2-x/2}Ge_{x/2}]$ puckered layer. (C) Y−Ga plane, viewed along the *c*-axis (left); an ordered model of the $Y_{0.67}Ga$ plane given for comparison (right).

via Ni−Ga(3) interactions at 2.477(2) Å to form a bilayer. The $[NiGa_{2-x/2}Ge_{x/2}]_2$ slabs then alternate with the $Y_{0.67}Ga$ planes as shown in Figure 3A. This structure type is related to that of $RE_{2-x}Pt_4Ga_{8+y}$, incidentally, also grown from Ga flux, although the latter has been refined in a different space group, $P\bar{3}1c$.[22]

In the disordered $Y_{0.67}Ga$ plane, unreasonably short distances are produced between the Ga(1) and Y atoms: Ga(1)−Ga(1) ∼ 1.6 Å and Y−Ga(1) ∼ 1.5 Å, owing to the symmetry equivalent positions of Y atoms at 2*c* ($^1/_3$ $^2/_3$ $^1/_4$) and Ga(1) atoms at 6*h* (*x* 2*x* $^1/_4$). Since such disorder does not represent a realistic picture of the atomic arrangement, partial occupancies of $^2/_3$ and $^1/_3$ were found for Y and Ga(1) sites, respectively.

Similar disorder between RE and Al atoms in the RE−Al plane was observed in the $RE_{2-x}Pt_4Ga_{8+y}$, $RENi_3Al_9$,[23] and $RE_4Pt_9Al_{24}$[24] family of compounds. As found by Gladyshevskii et al.,[23] the Y and Dy analogues of $RENi_3Al_9$ exhibit partially disordered arrangements of RE and Al atoms in a triangular mesh. In this case, the apparent distance between RE and Al in the Al_3 triangle was reported to be ∼1.5 Å. Interestingly, the Er and Gd analogues show an ordered arrangement with regular interatomic distances. Following the description given by Gladyshevskii, it is easy to model an ordered atomic arrangement from the disordered $YGa(1)_3$ plane by removing $^1/_3$ of the Y atoms and $^2/_3$ of the Ga(1) atoms: $Y \times {}^2/_3 + Ga(1)_3 \times {}^1/_3 = Y_{0.67}Ga(1)$; see Figure 3C. Thus, if every third Y atom is removed and the three Ga atoms that surround the remaining Y atom are also removed, as shown on the right side of Figure 3C, one obtains a perfectly ordered structure with reasonable Ga(1)−Ga(1) bond distances of about 2.5 Å. This larger unit cell is now characterized by a lattice parameter $a' = a\sqrt{3}$, where *a* is the parameter of the original subcell. The partial occupancies of $^2/_3$ and $^1/_3$ found for the Y and Ga(1) atoms of **1**, respectively, point to the validity of the given model. This exact type of arrangement, with an $a\sqrt{3}$ supercell, was observed in the ordered $GdNi_3Al_9$, in $ErNi_3Al_9$, and in $SmNi_3Ga_9$.[25] A similar ordered arrangement was reported by Thiede[24] et al. for $Er_4Pt_9Al_{24}$ described in a triclinic (space group $P\bar{1}$) supercell.

Despite these indications, numerous cell refinements using the collected X-ray data, performed on a number of analogues of **1,** failed to prove the existence of a proper $a\sqrt{3} \times a\sqrt{3} \times 3c$ superstructure. However, long-exposure zone photographs (*hk*0, 0*kl*, *h*0*l*) recorded on various crystals shed considerable light on the nature of the disorder and the presence of a $a\sqrt{3} \times a\sqrt{3}$ superstructure and provided useful information in understanding the mechanism of the crystal structure formation of this phase. Two features of the zone photographs are of extreme importance. First, in the *hk*0 zone photograph, the reflection spots do indeed correspond to a $a\sqrt{3} \times a\sqrt{3}$ supercell of 7.1864(7) Å; see Figure 4A. This diffraction pattern shows that the true cell (in the *ab* plane) is three times larger than the original one, and hence, the arrangement of RE and Ga atoms in the plane may in fact be ordered. Second, the

(21) Sieve, B.; Chen, X. Z.; Cowen, J.; Larson, P.; Mahanti, S. D.; Kanatzidis, M. G. *Chem. Mater.* **1999**, *11*, 2451.

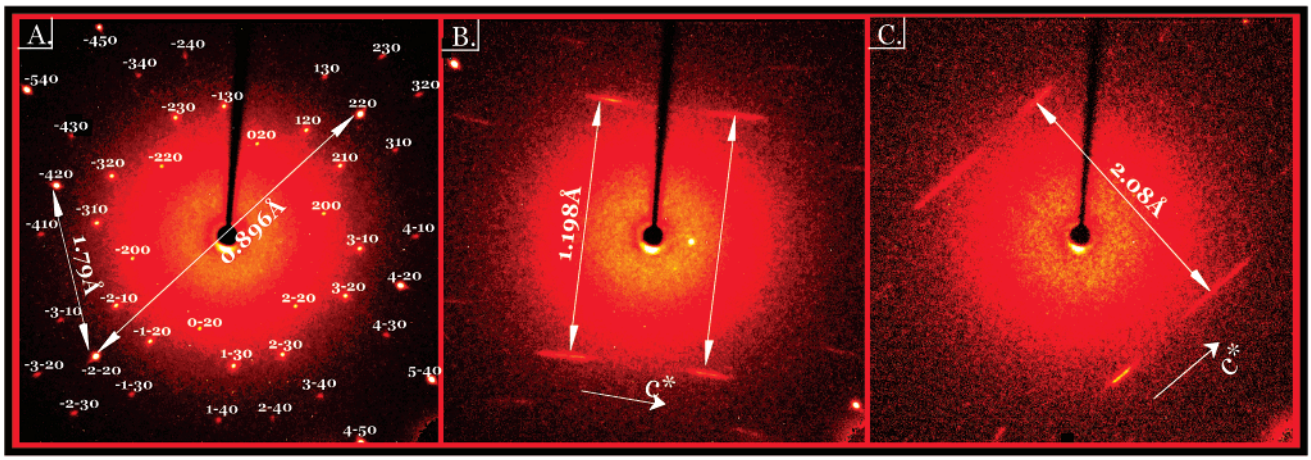

Figure 4. Zone photographs of $Ho_{0.67}Ni_2Ga_{5-x}Ge_x$: (A) *hk*0 zone (indexing of Bragg spots is given in the $a\sqrt{3} \times a\sqrt{3}$ supercell); (B) *h*0*l* zone; (C) 0*kl* zone. The exposure time is 360 s.

*h*0*l* and 0*kl* zone photographs, shown in Figure 4B and C, reveal diffuse scattering and streaking along the *l*-direction instead of regularly spaced discrete Bragg reflection spots. The observed streaks along the *c**-axis of the reciprocal unit cell are indicative of irregular nonperiodic stacking of $RE_{0.67}Ga$ planes along the *c*-axis. In other words, the *c*-axis of the unit cell can be viewed as infinitely large, so that the zero-dimension reflection spots are replaced with grossly elongated diffuse lines. Therefore, we conclude that the disorder seen from diffraction experiments originates in the extensive and random stacking faults of *ordered* $RE_{0.67}Ga$ planes (with a $a\sqrt{3} \times a\sqrt{3}$ supercell) along the direction of the *c*-axis.[23] Alternatively, we can state that the $RE_{0.67}Ga$ planes appear to be sliding easily along the *ab* plane, creating stacking disorder along the *c*-axis. The statistical averaging of the randomly stacked planes results in a smaller unit cell (the one shown in Table 1) and the observed disordered averaged picture. Thus, the description of the $YGa(1)_3$ plane emerging from the refinement seems to be the result of a "folding over" or "projecting" of the real structure onto a smaller unit cell.

The local coordination environments of Y, Ni, Ga(3), and M(2) = Ga/Ge types of atoms are shown in Figure 5 (the disorder M(1) types of atoms were excluded). The Y atoms are in the center of a bicapped trigonal prism, formed by six M(2) atoms and two Ga(3) atoms bonded at 3.049(1) and 3.264(2) Å, respectively. The Ni atoms are linked to the six-membered ring consisting of M(2) and Ga(3) atoms in a chair conformation. The bond distances from the central Ni atom to M(2) and Ga(3) are 2.4445(7) and 2.6151(9) Å, respectively. The Ni atom has an additional Ni−Ga(3) bond out of the $[NiGa_{2-x/2}Ge_{x/2}]$ puckered layer (Ni−Ga(3) = 2.477(2) Å), which connects two $[NiGa_{2-x/2}Ge_{x/2}]$ slabs into a double-layer. The M(2) atoms are bonded to a $Ni_3Ga(3)_3$ six-membered ring, with an M(2)−Ga(3) distance of 2.790(1) Å. The Ga(3) site is found in a cage of 10 atoms and is connected to an $Ni_3M(2)_3$ six-membered ring, and also capped with an $NiGa(3)_3$ "umbrella"; see Figure 5. The Ga(3)−Ga(3) bond distance is 2.824(2) Å.

Crystal Structure of 2: ($Gd_{0.67}Ni_2Ga_{6-x}Ge_x$; $Sm_{0.67}Ni_2Ga_{6-x}Si_x$; $Dy_{0.67}Ni_2Ga_{6-x}Ge_x$; $Y_{0.67}Co_2Ga_{6-x}Ge_x$). The structure of **2** is even more complicated than that of **1** in terms of the disorder taking place in the $RE_{0.67}Ga$ plane. Two crystal structures differing in the degree

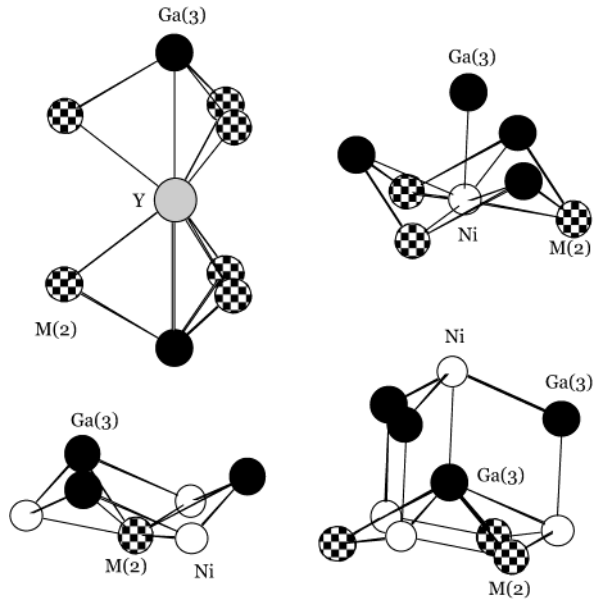

Figure 5. Local coordination of Y, Ni, Ga, and Ga/Ge atoms, in the structure of $Y_{0.67}Ni_2Ga_{5-x}Ge_x$. The disordered Ga(1) atoms are omitted for clarity.

of order in this plane were found in the analogues of **2**. For instance, in the case of RE = Y, Sm, and Gd, a satisfactory solution in the $P\bar{6}m2$ hexagonal space group was found. The structure of the Co analogue $Y_{0.67}Co_2Ga_{6-x}Ge_x$ of **2** was studied and refined by neutron diffraction, and is depicted in Figure 6; the atoms Y, Co, Ga, and M(2) = Ga/Ge are drawn analogously to those in **1**.

Similar to that of **1**, the crystal structure of **2** can be represented as a stacking of alternating $Ga[CoGa_{2-x/2}Ge_{x/2}]_2$ thick slabs and $Y_{0.67}Ga$ planes along the long (*c*) axis; see Figure 6A. The thick slab consisting of Co, Ga, and Ge atoms is reminiscent of the $[NiGa_{2-x/2}Ge_{x/2}]_2$

(22) Lacerda, A.; Canfield, P. C.; Beyermann, W. P.; Hundley, M. F.; Thompson, J. D.; Sparn, G.; Fisk, Z.; Burns, C.; Barnhard, A. C.; Lawson, A. C.; Kwei, G. H.; Goldsotne, J. *J. Alloys Compd.* **1992**, *181*, 191.
(23) Gladishevskii, R. I.; Cenuzal, K.; Flack, H. D.; Parthé, *Acta Crystallogr.* **1993**, *B49*, 468.
(24) Thiede, V. M.; Fehrmann, B.; Jeitschko, W. *Z. Anorg. Allg. Chem.* **1999**, *625*, 1417.
(25) Small, P.; Rangan, K. K.; Kanatzidis, M. G. Unpublished results.

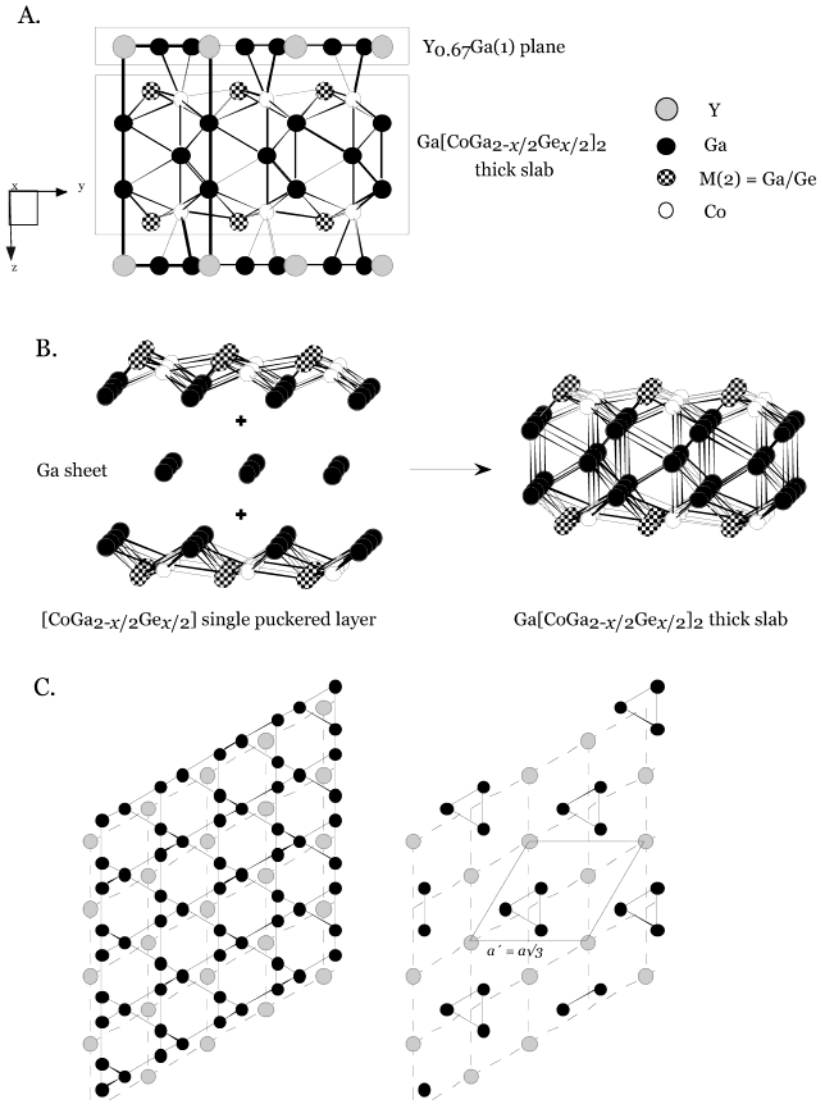

Figure 6. Structure of $Y_{0.67}Co_2Ga_{6-x}Ge_x$: (A) view along the *b*-axis; (B) the thick $Ga[CoGa_{2-x/2}Ge_{x/2}]_2$ slab as a combination of a Ga sheet sandwiched between two single $[CoGa_{2-x/2}Ge_{x/2}]$ puckered layers; (C) the Y−Ga plane, viewed along the *c*-axis (left); an ordered model of the $Y_{0.67}Ga$ plane given for comparison (right).

double-puckered layer in **1**. The difference lies in the thickness of the layer and the way the single-puckered layers are oriented against each other. As shown in Figure 6B, the $Ga[CoGa_{2-x/2}Ge_{x/2}]_2$ thick slab is constructed of two single-puckered layers, identical to those of **1**, but this time an additional Ga sheet is sandwiched between them. The two puckered layers in **2** are related to each other by mirror symmetry (the mirror plane contains the extra Ga sheet), and connected via Ga atoms (Ga(3)−Ga(3) = 2.781(2) Å) and through Co atoms bonded to the Ga(4) atoms of the Ga sheet (Co−Ga(4) = 2.366(3) Å). In **1**, the puckered layers in addition to the mirror symmetry are rotated 60° with respect to each other.

The $Y_{0.67}Ga$ planes in the structure of **2** are identical to those found in **1**. A similar type of disorder between Y and Ga(1) atoms is observed; see Figure 6C. As was discussed above, the ordered arrangement (with the supercell parameter $a' = a\sqrt{3}$) of Y and Ga atoms in the plane can be achieved if $^1/_3$ of the Y atoms and $^2/_3$ of the Ga atoms were removed. We point out once more that, although the existence of an ordered structure with a $a\sqrt{3} \times a\sqrt{3} \times 3c$ supercell was found for isotypic ternary phases such as $RENi_3Al_9$ and $RENi_3Ga_9$, we could not observe an ordered arrangement in any analogues of **2**.

As was discussed for **1**, such disorder can derive from the high degree of stacking faults of the $Y_{0.67}Ga$ planes in the direction of the *c*-axis. Justification of this argument is found particularly in the *hk*0 and *0kl* zone photographs of **2** (RE = Dy, Tt = Ge); see Figure 7. Whereas the indexing of the *hk*0 zone reflections clearly corresponds to a supercell of $a' = a\sqrt{3}$, the *0kl* and *h0l* zone photos reveal considerable diffuse scattering along the reciprocal *c**-axis. Thus, the disorder found in the two homologous compound types **1** and **2** is of the same origin.

The local coordination environments of Y, Co, Ga, and M(2) atoms are depicted in Figure 8. The disordered M(1) atoms are omitted for clarity. The Y atoms are in the center of the trigonal prism formed by six M(2) atoms (the Y−M(2) bond distance is 3.0509(8) Å) and two Co atoms (Y−Co = 3.230(1) Å). The Co atoms are seven-coordinate and are bonded to three Ga(3) and three M(2) atoms of the puckered layer and to one Ga(4) atom of the Ga sheet at 2.366(3) Å. The atoms on

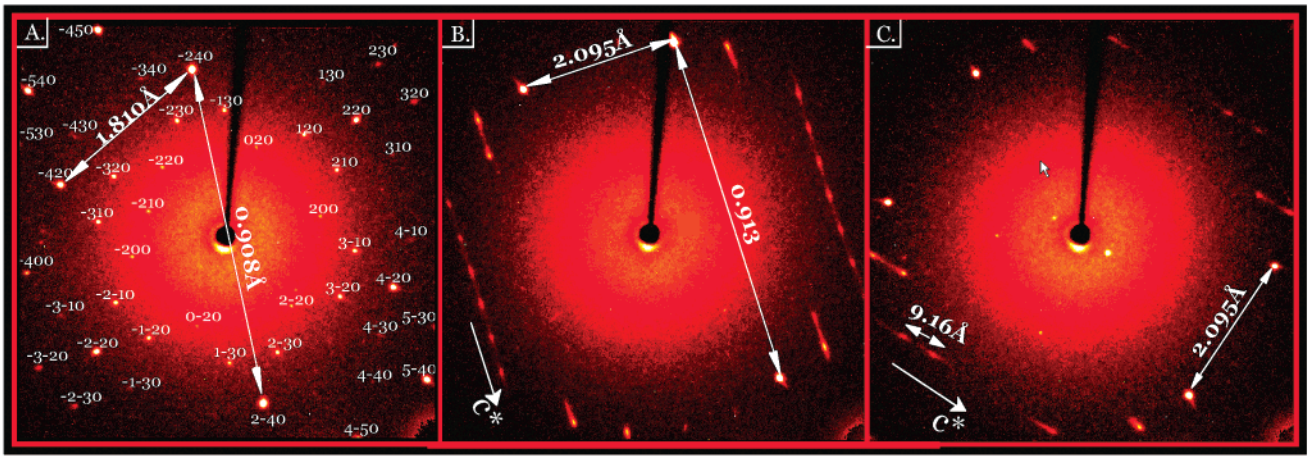

Figure 7. Zone photographs of $Dy_{0.67}Ni_2Ga_{6-x}Ge_x$: (A) *hk*0 zone (indexing of the individual Bragg spots is given in the $a\sqrt{3} \times a\sqrt{3}$ supercell); (B) *h*0*l* zone; (C) *0kl* zone. The exposure time is 360 s.

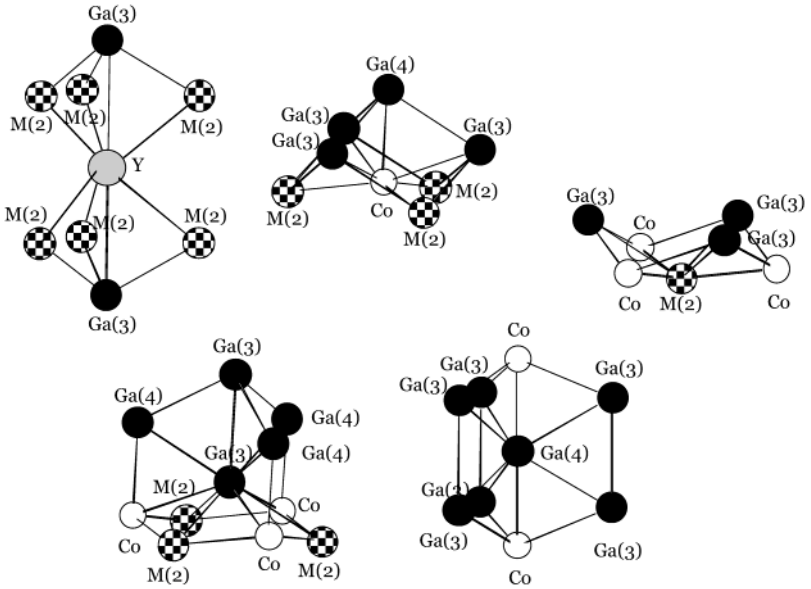

Figure 8. Local coordination of Y, Co, Ga, and Ga/Ge atoms in the structure of $Y_{0.67}Co_2Ga_{6-x}Ge_x$. The disordered Ga(1) atoms are omitted for clarity

the mixed-occupancy M(2) site, being part of the puckered layer, are connected to three Co atoms and to three Ga(3) atoms at the distances 2.4458(5) and 2.7735(7) Å, respectively. The Ga(3) atoms are ten-coordinate; they are self-bonded at 2.781(2) Å and also connected to three Ga(4) atoms of the Ga sheet at 2.7864(6) Å to link two puckered layers. The Ga(3) coordination environment includes another six atoms: three Co atoms at 2.604(1) Å and three M(2) atoms. The bicapped trigonal prism of two Co atoms and six Ga(3) atoms comprises a coordination polyhedron of Ga(4) atoms.

Although a single-crystal sample exhibiting an ordered superstructure could not be found in **2**, samples of the Dy analogue appeared to be more ordered, showing an average structure that is intermediate between the substructure and the superstructure, and exhibiting partial ordering in the $RE_{0.67}Ga$ plane. For instance, the $Dy_{0.67}Ni_2Ga_{6-x}Ge_x$ crystallizes in a primitive hexagonal cell with parameters $a'' = a\sqrt{3} = 7.2536(8)$ Å and $c'' = 2c = 18.308(3)$ Å. The obtained cell relates to the subcell parameters (a, c) as $a\sqrt{3} \times a\sqrt{3} \times 2c$ and to the supercell parameters (a', c') as $a' \times a' \times {}^2/_3c'$. The fully ordered superstructure unit cell, as it is for example for $ErNi_3Al_9$, has $a' = 7.2716(5)$ Å and $c' = 27.346(3)$ Å. Thus, this structure is an intermediate between the substructure and the superstructure. The crystallographic result of this is a partial order in the RE−Ga(1) planes. The drawing of the RE−Ga plane of the Dy analogue of **2** is depicted in Figure 9 (center), and the RE−Ga planes of the substructure and the superstructure are given for comparison to the left and to the right, respectively. It is obvious from Figure 9 that the central fragment depicting the Dy−Ga plane can be obtained from the disordered plane shown on the left-hand side by removing the Ga atoms from around half of the Dy atoms. Those Dy atoms (Dy(1) in the supercell notation) are therefore ordered (do not have any atoms at short distances). The remaining half of the Dy atoms (Dy(2)), are still disordered; that is, three Z(2) atoms are bonded to every Dy(2) atom at very close distance, defining a triangle. Likewise, Ga(1) atoms have Z(1) atoms in the center of the triangle which create short distances. If both Z(1) and Z(2) disordered atoms are removed, the ordered arrangement appearing on the right of Figure 9 is obtained.

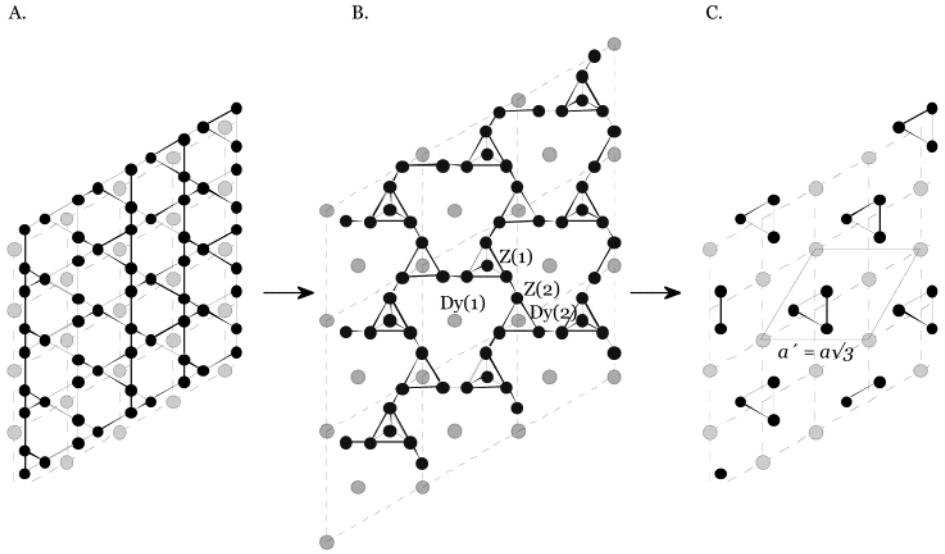

Figure 9. Dy−Ga plane with partial disorder, as found in $Dy_{0.67}Ni_2Ga_{6-x}Ge_x$ (center); RE−Ga(1) plane with complete disorder, as found in $RE_{0.67}Ni_2Ga_{5-x}Ge_x$ (left); and ordered RE−Al plane, as observed in the $ErNi_3Al_9$ structure type (right), given for comparison.

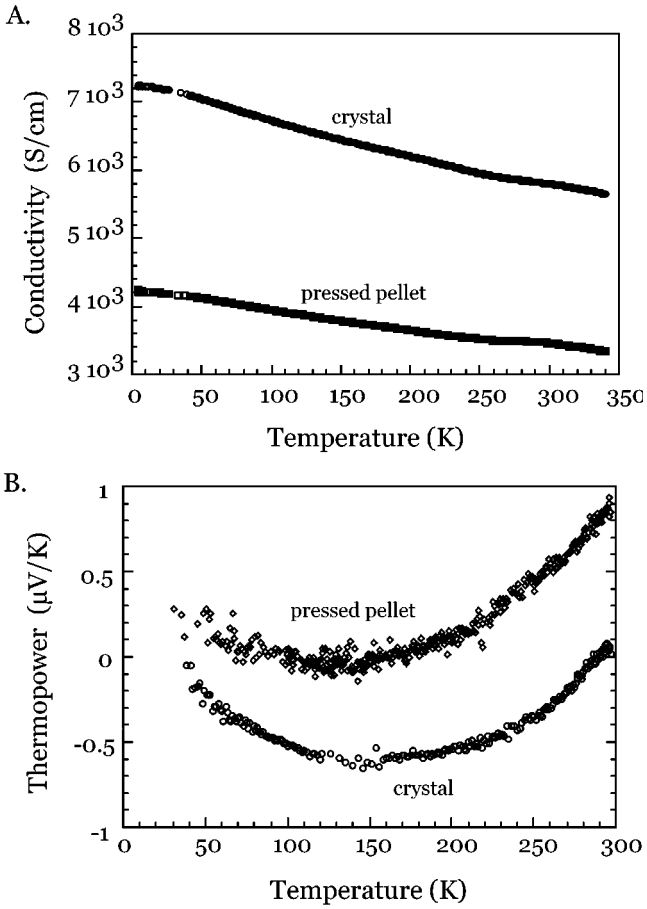

Figure 10. (A) Electrical conductivity and (B) thermopower measurements as a function of temperature for $Sm_{0.67}Ni_2Ga_{5-x}Ge_x$.

Transport Properties. Electrical conductivity and thermopower measurements were performed on single-crystal and polycrystalline samples (pressed into pellets) of $Sm_{0.67}Ni_2Ga_{5-x}Ge_x$; see Figure 10. The room-temperature conductivity is ∼6000 S/cm for a single-crystal sample and ∼3500 S/cm for a pressed pellet. The temperature dependence of the electrical conductivity (σ) has a negative slope of the dσ/dT curve, which, coupled with the very low values of the thermoelectric power, indicates high metallic character.

Magnetic Properties. Because of the explicit rodlike morphology and the large crystal size of compounds **1** and **2**, we were able to study the magnetic response to an applied external magnetic field as a function of temperature in single-crystal samples. Measurements on polycrystalline samples were also performed. Six analogues of **1** (RE = Y, Gd, Tb, Ho, Er, Tm) and two analogues of **2** (RE = Dy, and RE = Y with M = Co) with Ge were used for the measurements. The results are summarized in Table 11 and Figures 11−13.

The temperature dependence of the molar magnetic susceptibility χ_m (calculated per mole of RE) is shown in Figure 11. At low temperatures (3−4 K, see inset), a well-pronounced χ_m maximum occurs for RE = Gd, Tb, and Er. In the case of Dy, two maxima at about 10 and 3.5 K were observed. The RE = Ho and Tm analogues, however, show no T_{max}, which presumably lies at temperatures below 2 K and outside of our experimental limits. Below the T_{max}, some analogues such as Tb display irreversibility in the field-cooled (FC) and zero-field-cooled (ZFC) susceptibility. The ZFC part of χ_m is decreasing rapidly as the temperature drops below the T_{max}, while the FC part of χ_m continues to rise even below T_{max}. The maxima on the χ_m-T plots indicate possible anti-ferromagnetic ordering taking place at temperatures below T_{max}.

At higher temperatures, the thermal energy becomes sufficient to disrupt the alignment of the magnetic moments, and the system falls into a paramagnetic state. The Curie law is obeyed in the isotropically averaged polycrystalline magnetic susceptibility $\chi^{iso}{}_m$, while anisotropic $\chi^{||c}{}_m$ and $\chi^{\perp c}{}_m$ exhibit Curie−Weiss behavior with the Weiss constant Θ ranging from −66 to +26 K. The characteristic plots of $\chi_m{}^{-1}$ versus T are shown in Figure 12. The effective magnetic moments (μ_{eff}) for different rare-earth analogues calculated from the linear part of the $\chi_m{}^{-1}$ versus T plot were found to be very close to the values expected for the free RE^{3+} ions.[26] Thus, the contribution to the magnetic susceptibility of these systems is due solely to the rare-earth

Table 11. Summary of Magnetic Results for $RE_{0.67}Ni_2Ga_{5+n-x}Ge_x$

	$Gd_{0.67}Ni_2Ga_{5-x}Ge_x$			$Tb_{0.67}Ni_2Ga_{5-x}Ge_x$			$Dy_{0.67}Ni_2Ga_{6-x}Ge_x$			$Ho_{0.67}Ni_2Ga_{5-x}Ge_x$			$Er_{0.67}Ni_2Ga_{5-x}Ge_x$			$Tm_{0.67}Ni_2Ga_{5-x}Ge_x$		
	H^{iso}	$H\|\|c$	$H\perp c$	H^{iso}	$H\|\|c$	$H\perp c$	H^{iso}	$H\|\|c$	$H\perp c$	H^{iso}	$H\|\|c$	$H\perp c$	H^{iso}	$H\|\|c$	$H\perp c$	H^{iso}	$H\|\|c$	$H\perp c$
T_{max}[a] (K)	~3		~3		~3	~3				~3				~4	~3	~4		
Θ[b] (K)	−8	−7	+12	0	−66	−11	0	−56	0	0	−17	+6	0	+14	−11	0	+26	−34
$\Theta_{\|\|} - \Theta_{\perp}$[c] (K)					−55			−56			−23			+25			+60	
K_2^{para}[d] ($\times 10^{-15}$ erg/ion)					9.93			10.73			4.47			−4.20			−11.04	
$K_2°$[e] ($\times 10^{-15}$ erg/ion)					9.77			10.63			4.25			−4.79			−10.24	
μ_{eff}^{CW}[f] (μ_{BM})	7.79	7.90	8.30	7.28	9.64	9.86	10.8	11.1	10.8	9.31	10.6	10.4	11.1	9.60	9.97	9.90	7.79	7.85
μ_{eff}^{ave}[g] (μ_{BM})		8.00			9.60			10.93			10.7			9.82			7.64	
μ_{eff}^{calc}[h] (μ_{BM})		7.94			9.72			10.63			10.6			9.57			7.63	
μ_{eff}^{hys}[i] (μ_{BM})	~4	~4	~5	~6	~1.5	~6	~7	~2.5	~7	~6	~4	~9	~9	~9	~3	~8	~7	~3
easy axis[j]	isotropic			in BASAL plane			in BASAL plane			in BASAL plane			|| to *c*-axis			|| to *c*-axis		

[a] The temperature of the maximal magnetic susceptibility. [b] Paramagnetic Curie temperature (Weiss constant). [c] The difference between the paramagnetic Curie temperatures for field directions parallel and perpendicular to the *c*-axis. [d] Effective 0 K 2-fold anisotropy constant calculated from the paramagnetic Curie temperature anisotropy. [e] Theoretical values of the single-ion 2-fold anisotropy constant at 0 K. [f] The effective magnetic moment μ_{eff} calculated from the linear part of the reciprocal magnetic susceptibility vs temperature. [g] Averaged value of the isotropic and anisotropic values of μ_{eff}. [h] μ_{eff} calculated on the basis of the Van Vleck equation for free RE^{3+} ion. [i] The maximal effective magnetic moment μ_{eff} obtained from the field dependence curves. [j] The direction of the magnetically easy axis with respect to the crystallographic axis obtained from the onset of the M(H) saturation magnetization.

atoms which are in the +3 oxidation state, whereas the Ni atoms are in a nonmagnetic state. Additionally, the temperature dependence of magnetization of **1** for the nonmagnetic Y analogue was measured to probe the magnetic state of Ni atoms. The results are consistent with the nonmagnetic behavior of Ni and show a very small room-temperature magnetization of about 8.77×10^{-5} emu·mol^{-1} with a very weak temperature variation $d\chi_m/dT$ of -7.0×10^{-7} emu·mol^{-1}·K^{-1}. A similar diamagnetic behavior was observed for the Y analogue of **2** with Co ($\chi_m^{RT} = 7.50 \times 10^{-5}$ emu·mol^{-1}; $d\chi_m/dT = -8.6 \times 10^{-7}$ emu·mol^{-1}·K^{-1}), which supports the general idea that in these types of RE/M/T/Al(Ga) compounds the transition metals are in nonmagnetic states. The values of μ_{eff}, $\Theta_{||c}$, and $\Theta_{\perp c}$ for the isotropic and anisotropic measurements, as well as the average value of μ_{eff}, are given in Table 11.

The field dependence magnetization curves of **1** (RE = Gd, Tb, Ho, Er, and Tm) and **2** (RE = Dy) are shown in Figure 13. The Gd analogue of **1** has the only rare-earth ion in this series which does not have a contribution from the orbital momentum to the total momentum. Magnetization curves do not exhibit anisotropy effects up to fields of 5 T. The magnetization at 5 T reaches only 70% of its saturation value. In the case of Tb and Ho analogues of **1**, substantial basal plane anisotropy is observed (basal plane, or the *ab* plane lies perpendicular to the *c*-axis). Although at the fields H⊥*c* of 5 T only the onset of the saturation is observed, the direction perpendicular to the *c*-axis is the magnetically easy axis, and the magnetic moments are constrained to the basal plane. In the case of H||*c*, μ_{eff}^{hys} yields ~1.5 and ~4 μ_{BM} for Tb and Ho, respectively, which are about 15% and 40% of the saturation value. A similar situation is observed for the Dy analogue of **2**. A magnetic moment of ~7 μ_{BM} (70% of saturation value) is developed at 5 T when the applied magnetic field is directed parallel to the basal plane, and a magnetic moment of only ~2.5 μ_{BM} is developed if it is oriented parallel to the *c*-axis.

Unlike the case of the Tb and Ho analogues, the basal plane of Er and Tm is magnetically hard; that is, the easy axis does not lie in the basal plane. A moment of only ~3 μ_{BM} is developed in the basal plane in a 5 T field. However, an application of an external filed of only 1 T along the *c*-axis yields a full saturation moment of ~9 μ_{BM} for the case of Er, and ~7 μ_{BM} for the case of Tm. Thus, in these two cases, the [001] direction defines the magnetically easy axis.

The large magnetic anisotropy found in the analogues of **1** and **2** parallels the behavior observed in the heavy rare-earth metals[27] themselves. The latter has been attributed to the interaction of the Coulomb crystal field and the nonspherical 4*f* charge cloud distribution on the basis of the single-ion approximation. The effect of the crystal field is small compared to the exchange and is manifested as an anisotropy, that is, a tendency to align the charge clouds (and magnetic moments together with it) along the crystal axis. In a phenomenological form, the effect of the crystal field of hexagonal symmetry can be expressed as the potential[28,29]

$$V = A_2°\alpha\langle r^2\rangle Y_2°(\mathbf{J}) + A_4°\beta\langle r^4\rangle Y_4°(\mathbf{J}) + A_6°\gamma\langle r^6\rangle Y_6°(\mathbf{J}) + A_6^{\,6}\gamma\langle r^6\rangle Y_6°(\mathbf{J})$$

The numerical constants[30] α, β, and γ (Stevens' constants), the averages over the 4*f* wave functions $\langle r^l\rangle$, and the operator equivalents of spherical harmonics $Y_l^m(\mathbf{J})$ are the properties of free ion, while the electric field components A_l^m are properties of the crystal lattice. The magnetic anisotropy energy in terms of the anisotropy coefficients K_l^m and spherical harmonics $Y_l^m(\theta, \varphi)$ can be written as

$$E_K = K_2Y_2°(\theta, \varphi) + K_4Y_4°(\theta, \varphi) + K_6Y_6°(\theta, \varphi) + K_6^{\,6}Y_6^{\,6}(\theta, \varphi)$$

where θ and φ are the angles between the direction of the magnetic moment and the *c*- and *a*-axes, respectively. The K_l (i.e. K_2, K_4, K_6) uniaxial anisotropy is dominant in the pure heavy RE metals, and among these, the 2-fold anisotropy constant K_2 has the largest

(26) Van Vleck, J. H. *The Theory of Electric and Magnetic Susceptibilities*; Oxford University Press: Oxford, U.K., 1932.

(27) Elliot, R. J. In *Magnetic Properties of Rare Earth Metals*; Elliot, R. J., Ed.; Plenum Press: London and New York, 1972; pp 1−16.

(28) Rhyne, J. J. In *Magnetic Properties of Rare Earth Metals*; Elliot, R. J., Ed.; Plenum Press: London and New York, 1972; Chapter 4, pp 129−185.

(29) Elliot, R. J. *Phys. Rev.* **1961**, *124*, 346.

(30) Stevens, K. W. H. *Proc. Phys. Soc. (London)* **1952**, *A65*, 209. Elliot, R. J.; Stevens, K. W. H. *Proc. R. Soc. (London)* **1953**, *218*, 553.

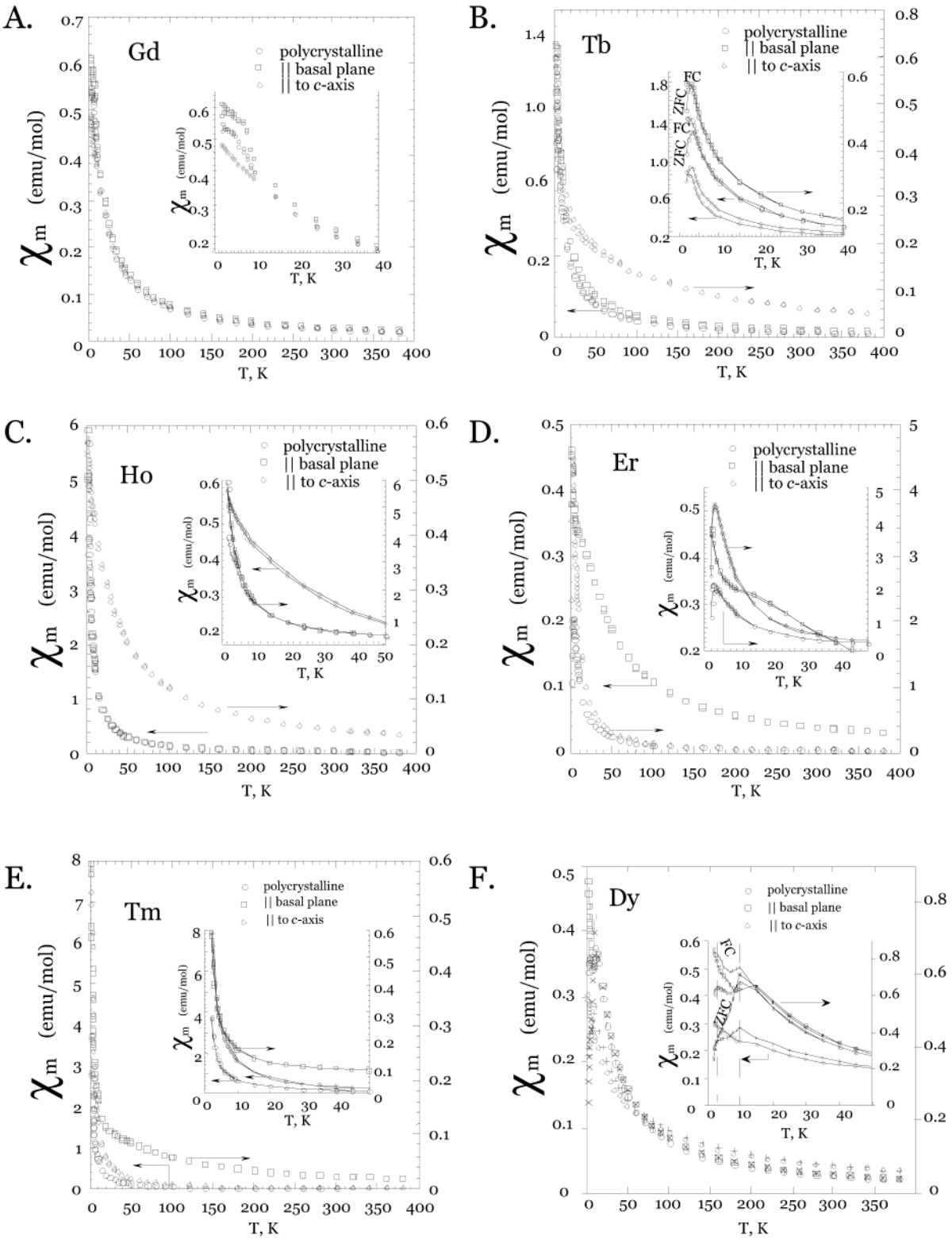

Figure 11. Temperature dependence of the molar magnetic susceptibility χ_m for single-crystal and polycrystalline samples of $RE_{0.67}Ni_2Ga_{5-x}Ge_x$ (RE = Gd, Tb, Er, Ho, Tm) and $RE_{0.67}Ni_2Ga_{6-x}Ge_x$ (RE = Dy); the low-temperature region is expanded in the inset at the upper right corner.

contribution to the anisotropy energy. Moreover, the magnitudes of K_2 scale approximately with the corresponding Stevens' constant α, while $A_2°$ and $\langle r^2 \rangle$ show only small variation in the heavy RE series.[28,31] The sign of α determines for the most part the direction of the anisotropy: α < 0 for Tb, Dy, and Ho, and the magnetically easy axis lies in the basal plane; α > 0 for Er and Tm, and the direction of the magnetically easy axis coincides with the *c*-axis of the hexagonal cell. In the case of Gd, which has an S ground state, α = 0, and as a consequence the single-ion contribution to the aniso-

(31) Kasuya, T. In *Magnetism*; Rado, G. T., Suhl, H., Eds.; Academic Press: New York, 1966; Vol. II B.

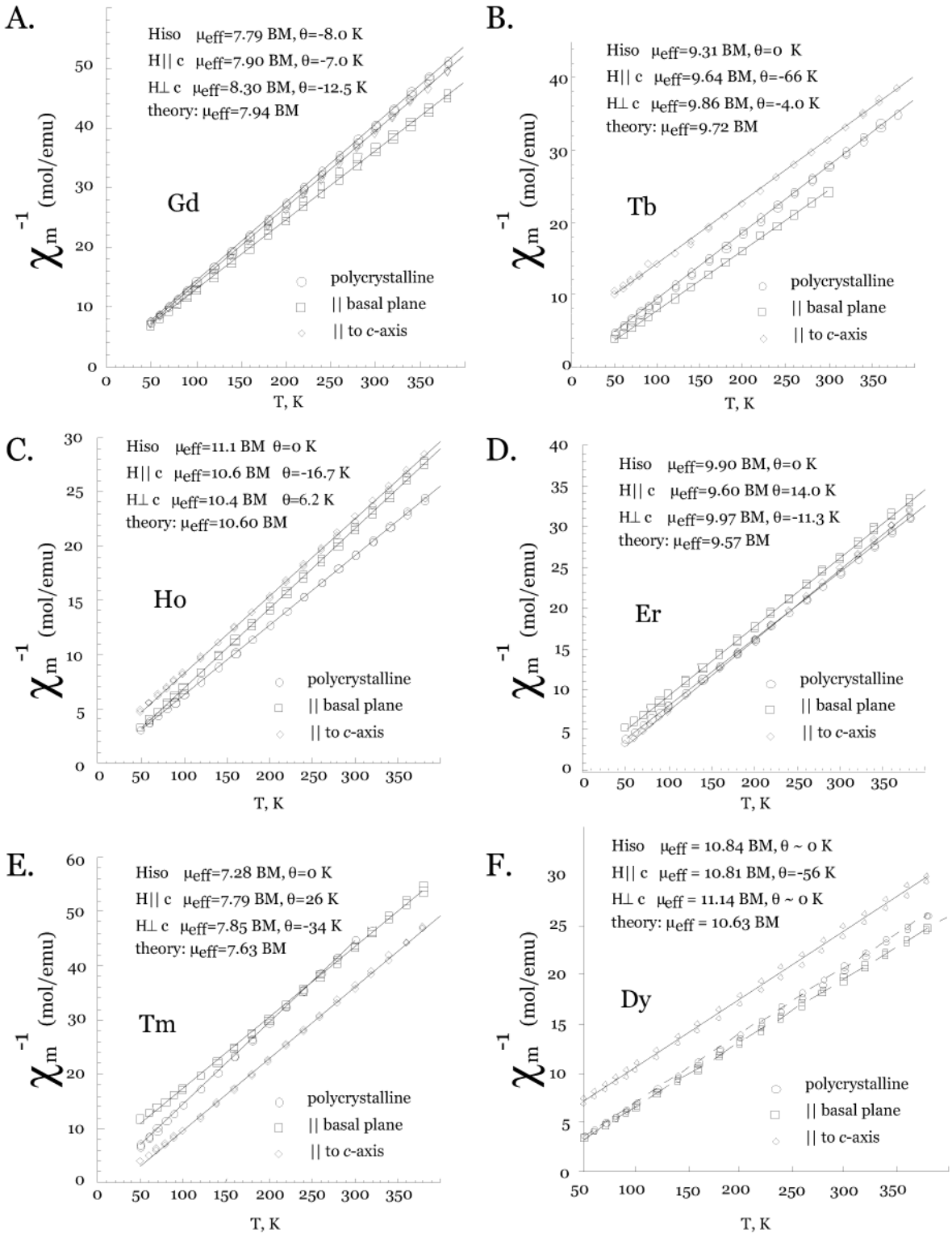

Figure 12. Linear part of the inverse molar magnetic susceptibility χ_m^{-1} for single-crystal and polycrystalline samples of $RE_{0.67}Ni_2Ga_{5-x}Ge_x$ (RE = Gd, Tb, Er, Ho, Tm) and $RE_{0.67}Ni_2Ga_{6-x}Ge_x$ (RE = Dy).

tropy vanishes, giving a nearly isotropic magnetization for Gd.

Because qualitatively similar results were obtained for the quaternary phases as for the pure RE metals,[27,28] we became interested in the magnitude of the magnetic anisotropy energy in these compounds, particularly in $K_2°$. Although the crystal structures of **1** and **2** are far more complicated than the close packed structures of elemental RE, the local coordination of the RE atoms is somewhat similar in both structures. Yet, even with the knowledge of the symmetry and the local environment of RE atoms in **1** and **2**, it is hard to apply a point charge model approximation in order to calculate the crystal field potential.[32] However, the anisotropy constant K_2^{para} can be obtained experimentally from the Weiss constant anisotropy $\Delta\Theta = \Theta_{||} - \Theta_{\perp}$ according to the equation[28] $k\Delta\Theta = 3[4J(J+1) - 3]K_2^{para}/10J(2J-1)$, where J is the total angular momentum and k is a

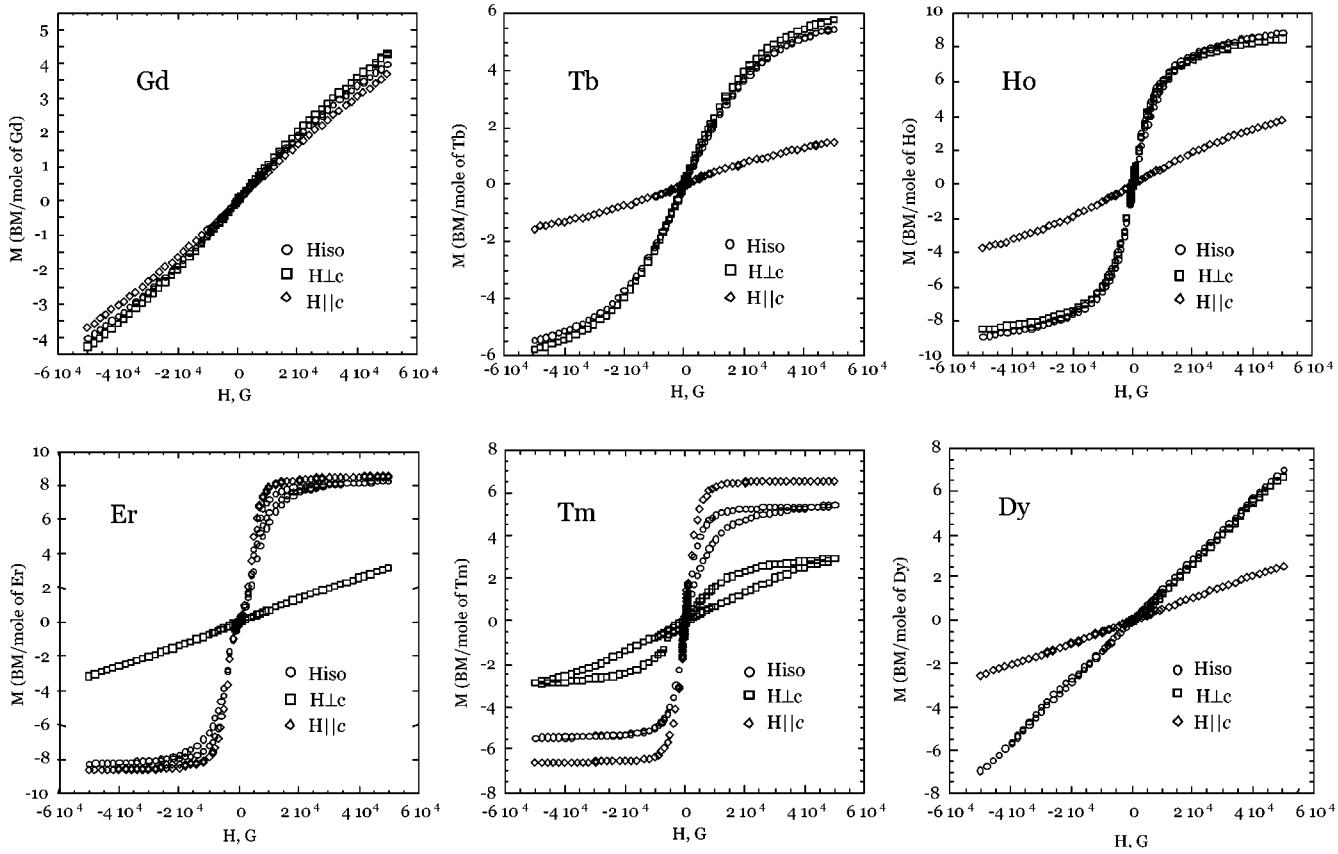

Figure 13. Anisotropic and isotropic field dependence magnetization curves (μ_{BM}/per RE ion) of $RE_{0.67}Ni_2Ga_{5-x}Ge_x$ (RE = Gd, Tb, Er, Ho, Tm) and $RE_{0.67}Ni_2Ga_{6-x}Ge_x$ (RE = Dy) measured at T = 2 K.

Boltzman constant. The values of K_2^{para} for the heavy RE analogues of **1** and **2** are listed in Table 11; the theoretical values of $K_2°$ calculated for heavy RE metals are given for comparison. The agreement between K_2^{para} and $K_2°$ is as surprising as it is striking, considering the large differences in the crystal structures between the quaternary phases described here and those of RE elements. It is plausible to consider that perhaps the strength of the interaction of the crystal field with the local magnetic moments is dictated primarily by the properties of the free rare-earth ion (α, $\langle r^l \rangle$, $Y_l^m(\mathbf{J})$) and only secondarily by the properties of the crystal field.

Conclusion

The exploratory reaction chemistry in the quaternary systems RE/Ni/Tt (where RE = Y, Sm, Dy, Gd, Tb, Er, Ho, and Tm; and Tt = Si or Ge) and RE/Co/Ge (with RE = Y or Gd) using liquid Ga led to two types of new intermetallic phases of the formula $RE_{0.67}Ni_2Ga_{5+n-x}Tt_x$, with $n = 0$ or 1. It was necessary to determine the distribution of Ga and Ge in these structures with single-crystal neutron diffraction, which revealed the location of Ge in a mixed occupancy site consisting of 67% Ga and 33% Ge. The structures of these phases are related and can be represented as a consequent stacking of the $RE_{0.67}Ga$ planes and $Ga_n[Ni_2Ga_{4-x}T_x]$ thick slabs along the *c*-axis. A persistent feature shared by all the phases is the disorder of the $RE_{0.67}Ga$ layer, where the atoms of RE and Ga form a triangular mesh with unreasonably close distances. The observed disorder is an average picture that emerges from the random and continuous stacking faults of ordered $RE_{0.67}Ga$ planes with a supercell of $a\sqrt{3} \times a\sqrt{3}$. The stacking irregularities do not allow an ordered structure to develop along the *c*-axis. On the basis of the diffraction properties of these crystals, an ordered arrangement of these planes was proposed.

Electrical conductivity and thermopower measurements show the metallic behavior of these compounds. The effective magnetic moments on the RE atoms obtained from the Curie temperature dependence indicate RE^{3+} atoms. A strong anisotropy with respect to the crystallographic axis was detected for these compounds. The field dependence measurements point out that the direction of the magnetically easy axis coincides with the *c*-axis for RE = Er, and Tm, and lies in the basal plane in the case of Tb, Dy, and Ho. The single-ion 2-fold anisotropy constants K_2^{para} calculated from the Weiss constant anisotropy are in good agreement with the theoretical ones calculated for the pure RE metals.

Acknowledgment. Financial support from the Department of Energy (Grant No. DE-FG02-99ER45793) is gratefully acknowledged. This work made use of the SEM/EDS facilities of the Center of Advanced Microscopy at Michigan State University. The work at Argonne National Laboratory was supported by the U.S. Department of Energy, Basic Energy Sciences-Materials Sciences, under Contract No. W-31-109-ENG-38.

(32) This is because a charge cannot be assigned to all elements in the compounds (except for RE, which has the charge +3).

Supporting Information Available: Tables of crystallographic details, atomic coordinates, and isotropic and anisotropic thermal displacement parameters for all atoms and interatomic distances and angles for $RE_{0.67}Ni_2Ga_{5-x}Si_x$ (RE = Tb); $RE_{0.67}Ni_2Ga_{5-x}Ge_x$ (RE = Y, Sm, Ho); $RE_{0.67}Ni_2Ga_{6-x}Si_x$ (RE = Sm); and $RE_{0.67}Ni_2Ga_{6-x}Ge_x$ (RE = Gd, Dy) (CIF). This material is available free of charge via the Internet at http://pubs.acs.org.

CM020066O